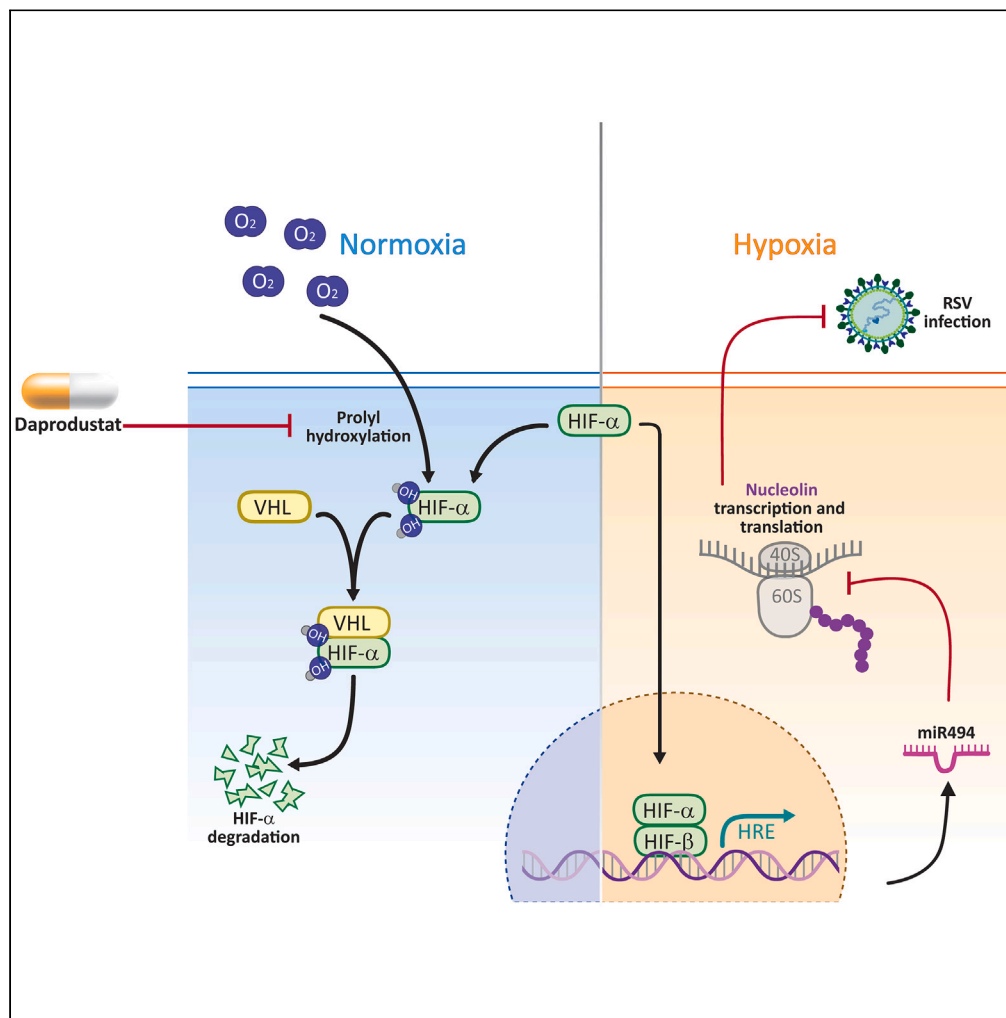


Article

Hypoxia inducible factors inhibit respiratory syncytial virus infection by modulation of nucleolin expression



Xiaodong Zhuang,
Giulia Gallo, Parul
Sharma, ..., James
P. Stewart, Dalan
Bailey, Jane A.
McKeating

xiaodong.zhuang@ndm.ox.ac.
uk (X.Z.)
jane.mckeating@ndm.ox.ac.uk
(J.A.M.)

Highlights

HIFs limit RSV cell-cell
fusion and replication

HIFs activate miR-494
which suppresses nucleolin
expression

HIF prolyl-hydroxylase
inhibitor limits RSV
infection in mice

HIFs suppress infiltrating
monocytes and neutrophils
in the lower respiratory
tract

Zhuang et al., iScience 27,
108763
January 19, 2024 © 2024 The
Authors.
[https://doi.org/10.1016/
j.isci.2023.108763](https://doi.org/10.1016/j.isci.2023.108763)

Article

Hypoxia inducible factors inhibit respiratory syncytial virus infection by modulation of nucleolin expression

Xiaodong Zhuang,^{1,8,*} Giulia Gallo,^{2,8} Parul Sharma,³ Jiyeon Ha,¹ Andrea Magri,¹ Helene Borrmann,¹ James M. Harris,¹ Senko Tsukuda,¹ Eleanor Bentley,³ Adam Kirby,³ Simon de Neck,⁴ Hongbing Yang,¹ Peter Balfe,¹ Peter A.C. Wing,⁵ David Matthews,⁶ Adrian L. Harris,⁷ Anja Kipar,^{3,4} James P. Stewart,^{3,9} Dalan Bailey,^{2,9} and Jane A. McKeating^{1,5,9,10,*}

SUMMARY

Respiratory syncytial virus (RSV) is a global healthcare problem, causing respiratory illness in young children and elderly individuals. Our knowledge of the host pathways that define susceptibility to infection and disease severity are limited. Hypoxia inducible factors (HIFs) define metabolic responses to low oxygen and regulate inflammatory responses in the lower respiratory tract. We demonstrate a role for HIFs to suppress RSV entry and RNA replication. We show that hypoxia and HIF prolyl-hydroxylase inhibitors reduce the expression of the RSV entry receptor nucleolin and inhibit viral cell-cell fusion. We identify a HIF regulated microRNA, miR-494, that regulates nucleolin expression. In RSV-infected mice, treatment with the clinically approved HIF prolyl-hydroxylase inhibitor, Daprodustat, reduced the level of infectious virus and infiltrating monocytes and neutrophils in the lung. This study highlights a role for HIF-signalling to limit multiple aspects of RSV infection and associated inflammation and informs future therapeutic approaches for this respiratory pathogen.

INTRODUCTION

Respiratory syncytial virus (RSV) causes lower respiratory tract illness in young children¹ and is increasingly recognised as a significant respiratory pathogen in immunocompromised adults and the elderly.² The virus is primarily transmitted through close contact, although it can spread via aerosolized droplets.³ Following a brief period of replication in the epithelium of the nasopharynx and upper respiratory tract, RSV can infect the small bronchioles or alveoli of the lower respiratory tract.⁴ Treatment options are limited and the humanized monoclonal antibody (Palivizumab) targeting the viral encoded fusion (F) protein is only used for passive immunoprophylaxis of high-risk infants.⁵ The recent FDA approval of RSV vaccines for immunizing elderly populations⁶ provides opportunities to reduce the burden of RSV associated disease and highlights the continued need to develop new anti-viral therapies for this infection.

During severe RSV infection, the host's immune response triggers an increase in mucus production and inflammation, leading to airway narrowing, bronchiolitis in young children and acute respiratory illness in the elderly or those with underlying chronic conditions.⁷ Virus induced damage to the alveolar epithelia can reduce local oxygen levels and is a common feature of RSV bronchiolitis that can result in respiratory failure, apnea, and death.^{8,9} Hypoxia inducible factors (HIFs) regulate the cellular transcriptome and metabolome in response to low oxygen and inflammatory conditions.¹⁰ HIF α subunits are regulated by oxygen-dependent pathways and when oxygen is abundant, newly synthesised proteins are hydroxylated by HIF prolyl-hydroxylase domain (PHD) enzymes and targeted for proteasomal degradation. When oxygen is limited the PHD enzymes are inactive and HIF α dimerizes with HIF-1 β to activate the transcription of genes regulating cell metabolism, pulmonary vasomotor control and immune regulation.^{11–13} HIF regulated genes can vary between cell types allowing a flexible and tissue specific response to diverse physiological signals.¹⁴

¹Nuffield Department of Medicine, University of Oxford, Oxford, UK

²The Pirbright Institute, Guildford, Surrey, UK

³Department of Infection Biology & Microbiomes, Institute of Infection, Veterinary and Ecological Sciences, University of Liverpool, Liverpool, UK

⁴Laboratory for Animal Model Pathology, Institute of Veterinary Pathology, Vetsuisse Faculty, University of Zurich, Winterthurerstrasse 268, 8057 Zurich, Switzerland

⁵Chinese Academy of Medical Sciences Oxford Institute, University of Oxford, Oxford, UK

⁶School of Cellular and Molecular Medicine, Faculty of Life Sciences, University of Bristol, Bristol, UK

⁷Oncology Department, University of Oxford, Oxford, UK

⁸These authors contributed equally

⁹Senior author

¹⁰Lead contact

*Correspondence: xiaodong.zhuang@ndm.ox.ac.uk (X.Z.), jane.mckeating@ndm.ox.ac.uk (J.A.M.)

<https://doi.org/10.1016/j.isci.2023.108763>



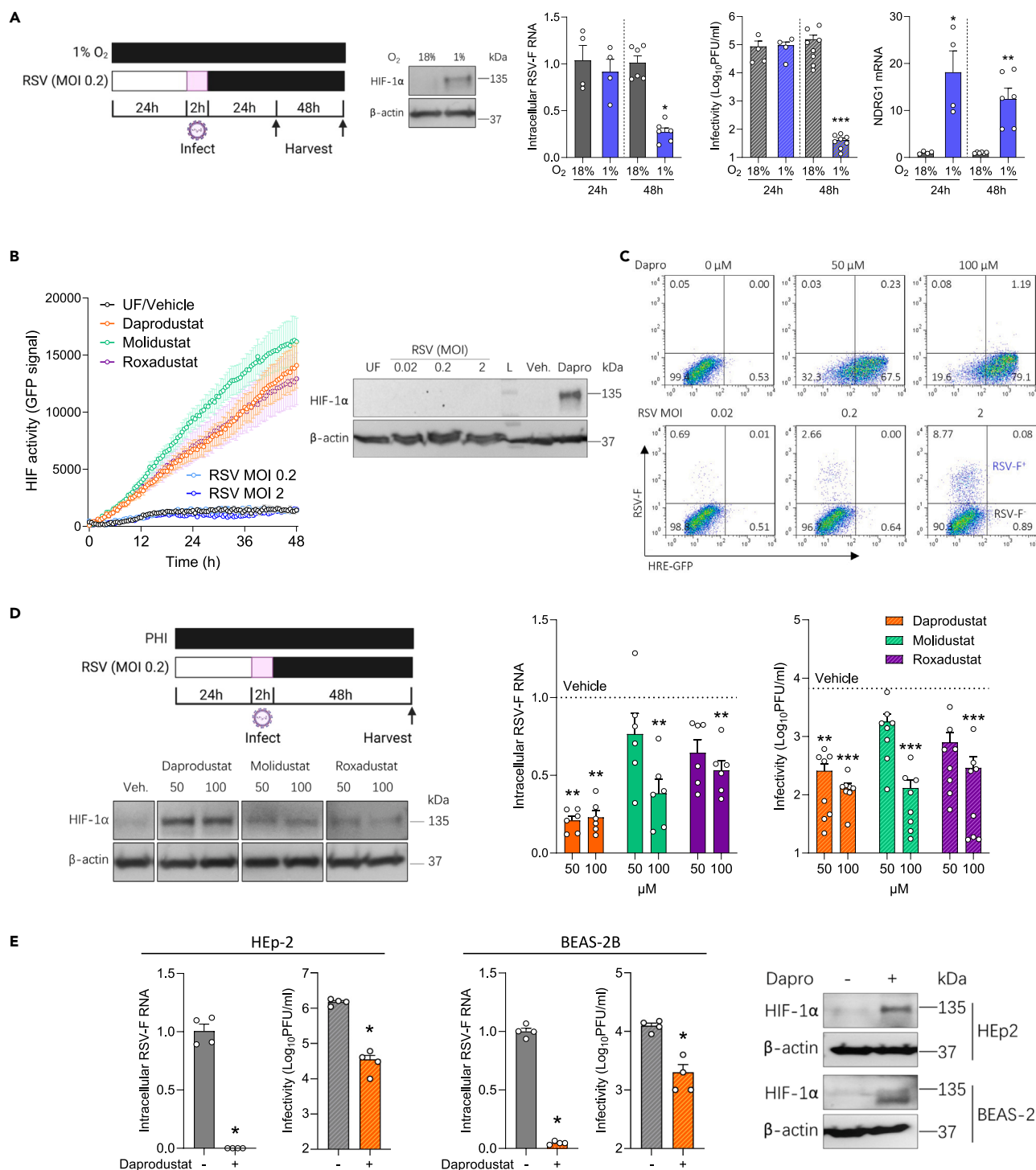


Figure 1. RSV infection is suppressed under hypoxic conditions and treatment with prolyl-hydroxylase inhibitors

(A) Calu-3 cells were cultured at 18% (gray) or 1% (blue) oxygen (O_2) for 24h prior to infecting with RSV (MOI 0.2) and the cultures maintained under normoxic or hypoxic conditions for the stated times and cells lysed for the PCR quantification of intracellular viral RNA (RSV-F), NDRG1 mRNA and infectivity at 24h or 48hpi (mean \pm SEM, $n = 4-8$, Mann-Whitney test, Two-sided). All data are expressed relative to 18% O_2 values at their respective time point. HIF-1 α and β -actin protein expression were assessed by immunoblot at 48hpi.

(B) Real-time monitoring of Calu-3 cells transduced with HRE-GFP were treated with PHIs (Daprodustat, Molidustat or Roxadustat at 50 μ M) or infected with RSV at MOI 0.2 or 2 (mean \pm SEM, $n = 5$), where UF = uninfected.

Figure 1. Continued

(C) Calu-3 HRE-GFP reporter cells were treated with Daprodustat at 50 or 100 μ M or infected with RSV at a range of MOIs for 48hpi and stained with anti-RSV-F-APC followed by flow cytometric analysis.

(D) Calu-3 cells were pre-treated with PHIs for 24h before infecting with RSV (MOI 0.2) and intracellular viral RNA (RSV-F) and infectivity measured at 48hpi (mean \pm SEM, $n = 6-8$, One-way ANOVA with multiple comparisons, Two-sided). HIF-1 α and β -actin protein expression were assessed by immunoblot at 48hpi.

(E) HEp-2 or BEAS-2B were pre-treated with Daprodustat (100 μ M) for 24h before infecting with RSV (MOI 0.2) and intracellular viral RNA (RSV-F) and infectivity measured at 48 hpi (mean \pm SEM, $n = 4$, Mann-Whitney test, Two-sided). HIF-1 α and β -actin protein expression were assessed by immunoblot at 48hpi. UF = uninfected. * denotes $p < 0.05$, ** < 0.01 and *** < 0.001 .

HIFs have been reported to enhance endogenous pathways to protect against lung injury during acute inflammation that include: promoting vascular repair;¹⁵ suppressing the inflammatory response in bronchial epithelial cells and reducing interleukin 6 and interferon gamma-induced protein 10 expression;¹⁶ regenerating alveolar type II pneumocytes;¹⁷ preventing the bioenergetic failure of alveolar epithelial cells during Acute Respiratory Distress Syndrome (ARDS)¹⁸⁻²⁰ and interacting with key metabolites such as succinate to limit damage from acute lung injury.²¹ Zhao et al. reported that lung epithelial *Hif1a* knockout mice support higher levels of influenza A virus infection and associated mortality.²² We previously reported that the hypoxic or pharmacological activation of HIFs limit SARS-CoV-2 infection and epithelial damage in the Syrian Golden Hamster model of COVID-19.^{23,24} Collectively, these studies highlight the significance of HIFs in defining host susceptibility to respiratory viruses and associated pathologies. Importantly this has the potential for pharmacological intervention since drugs inhibiting the PHD enzymes that drive HIF-mediated erythropoiesis are licensed for the treatment of renal anemia.²⁵⁻³⁰ These studies implicate HIF activation as a therapeutic strategy to combat lung injury.

RSV is primarily cell-associated and the virus can spread by cell-cell fusion, generating syncytia - large multinucleated cells formed by the fusion of infected with neighboring uninfected cells. The RSV fusion protein (RSV-F) has important roles in entry and fusion, driving particle attachment to cellular receptors and fusion of virion and host-cell membranes, either at the cell surface or during particle macropinocytosis.³¹ Several host factors including intercellular adhesion molecule 1 (ICAM1),³² epidermal growth factor receptor (EGFR)³³ and nucleolin (NCL)³⁴ have been shown to facilitate RSV mediated cell-cell fusion. In our study, we show that hypoxic conditions or treatment with PHD inhibitors (PHI) limits RSV infection via perturbing the expression of nucleolin via the hypoxia-induced microRNA, miR-494. Furthermore treatment of RSV infected mice with the clinically approved PHI, Daprodustat, reduced the level of infectious virus and infiltrating monocytes and neutrophils in the lung, highlighting a role for HIF-signalling in regulating host responses to respiratory viruses.

RESULTS

Hypoxia and HIF prolyl-hydroxylase inhibitors limit respiratory syncytial virus infection

To investigate a role for HIFs in regulating RSV replication we cultured human lung epithelial Calu-3 cells at 18% or 1% oxygen for 24h before infecting with RSV (A2 strain, MOI 0.2). Infection was quantified by measuring intracellular viral RNAs encoding fusion (F) and infectious virus at 24h and 48h post-infection (pi). We selected 1% oxygen as this is known to stabilise HIF α subunits and activate HIF target gene transcription. We confirmed the infected cells responded to hypoxia by immunoblotting for HIF-1 α and showed increased expression of the HIF regulated N-myc downregulated gene (NDRG1) expression (Figure 1A). Hypoxic conditions significantly reduced the level of RSV-F transcripts and infectious virus at 48hpi. Earlier studies showed that RSV infection stabilised HIF-1 α expression.³⁵⁻³⁷ To investigate whether RSV induced a functional HIF response in our model system, we used Calu-3 expressing a hypoxia-response element (HRE) driven GFP reporter. Treating the reporter cells with three PHIs (Daprodustat, Molidustat and Roxadustat) induced GFP expression in a time-dependent manner, whereas infection with RSV failed to activate GFP expression or to stabilise HIF-1 α expression (Figure 1B). Furthermore, flow cytometric analysis to identify infected cells showed no evidence of increased GFP expression in the RSV-F expressing cells, demonstrating that infection does not activate HIF signaling in Calu-3 cells. We confirmed the majority of Calu-3 cells (>70%) expressed GFP following Daprodustat treatment demonstrating the cells were responsive to PHI treatment (Figure 1C).

To ascertain a role for HIFs in regulating RSV infection, we treated Calu-3 cells with PHIs for 24h prior to infecting with RSV and demonstrated reduced levels of RSV-F transcript and infectious virus at 48hpi with no discernable effect on cell viability (Figures 1D and S1). HIF-1 α was detected in the PHI treated cells, with Daprodustat inducing the highest expression (Figure 1D). Kinetic analysis of Daprodustat treated Calu-3 cells showed a time-dependent expression of HIF-1 α and induction of NDRG1 gene expression at 24-48h post-treatment (Figure S2). To assess whether Daprodustat limits RSV replication/transcription we used a transient RSV replicon assay encoding a luciferase reporter.³⁸ RSV-driven luciferase activity was dependent on the viral encoded polymerase and Daprodustat reduced RSV replication (Figure S3). Viral RNA synthesis occurs in cytoplasmic inclusion bodies (IBs) that represent condensates of the viral replicase components formed by liquid-phase separation.³⁹ The steroidal alkaloid Cyclopamine was recently identified to target these IBs and limit viral replication and we demonstrated a potent inhibition of RSV-luciferase activity, consistent with the genesis of IBs in the RSV replicon assay (Figure S3). The antiviral activity of Daprodustat was replicated in two additional cell lines (HEp-2 and BEAS-2B) that are commonly used in RSV research⁴⁰ and we noted a reduction in intracellular RSV-F transcripts and infectious virus (Figure 1E). Probing the Daprodustat or vehicle treated RSV infected cell lysates for HIF-1 α confirmed expression in the drug treated cells (Figure 1E). We extended these observations to differentiated human primary bronchial epithelial cells (PBEC) propagated under air-liquid interface (ALI) and showed that Daprodustat reduced the level of infectious RSV secreted from the apical surface of these cultures (Figure S4). We only detected HIF-1 α expression or increased NDRG1 gene expression in the drug-treated ALI-PBEC, suggesting minimal evidence for RSV infection to activate HIFs in these model systems. Our previous

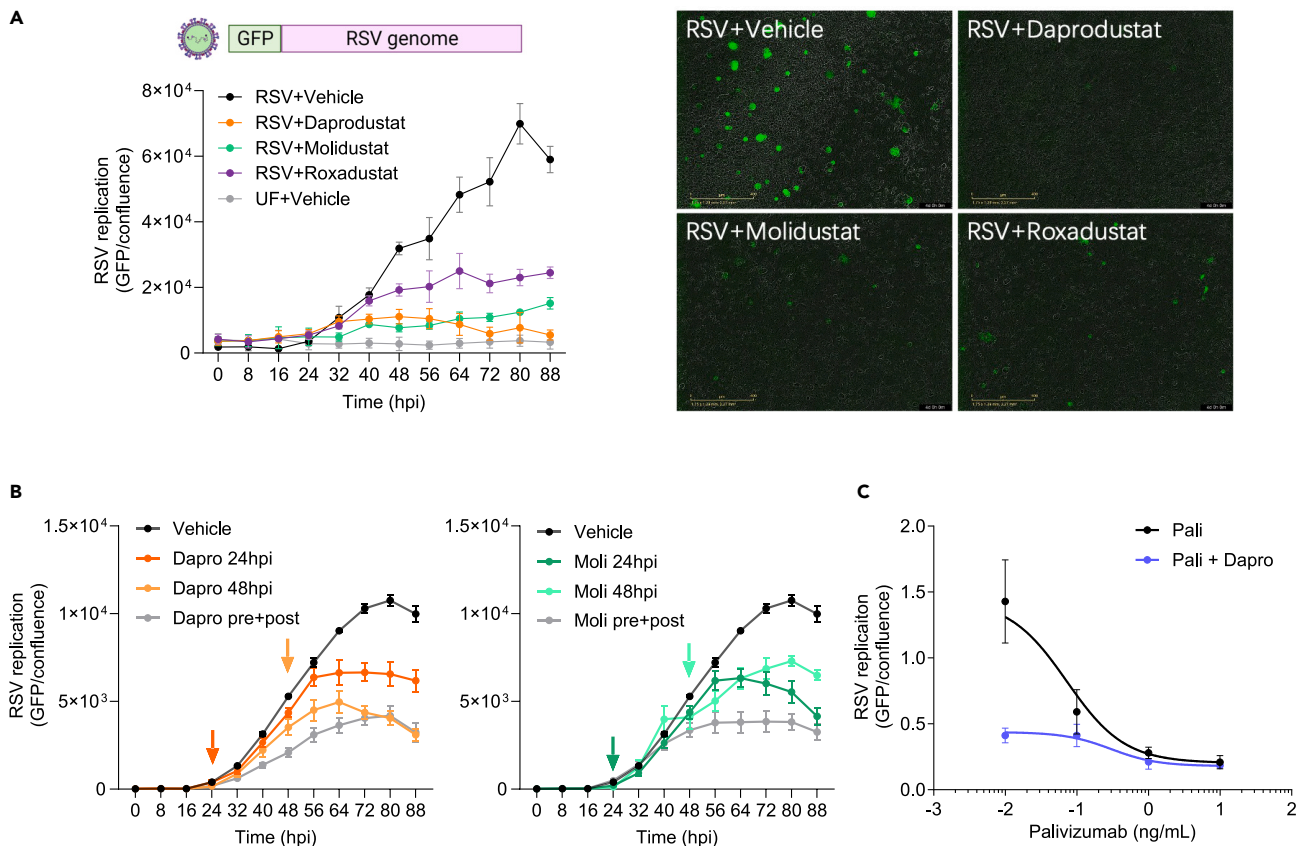


Figure 2. Prolyl-hydroxylase inhibitors inhibit RSV replication

(A) Calu-3 cells were pre-treated with PHIs (Daprodustat, Molidustat, Roxadustat at 50 μ M) 24h prior to infection with a reporter RSV expressing GFP (MOI 0.2) and viral replication measured every 8h using an Incucyte Live-Cell Imaging System. GFP signal was normalised per image with respect to cell confluence (mean \pm SEM, n = 4).

(B) Effect of PHI treatment on RSV infected Calu-3 cells. Calu-3 cells were treated with Daprodustat or Molidustat (50 μ M) before and after infection (pre+post) or 24hpi or 48hpi where the arrows indicate the addition of drugs and GFP expression measured using the Incucyte Live-Cell Imaging System. GFP signal and confluence were measured and the integrated intensity values are represented (mean \pm SEM, n = 6).

(C) Combined Daprodustat and Palivizumab treatment inhibits RSV replication. Calu-3 cells were treated with a range of Palivizumab doses in the presence or absence of Daprodustat (9.0 μ M) prior to infection with RSV-GFP (MOI 0.2) and viral replication measured at 48hpi using an Incucyte Live-Cell Imaging System. GFP signal was normalized per image and cell confluence (mean \pm SEM, n = 4). UF = uninfected.

experience of working with ALI-PBECs show limited HIF-1 α expression under laboratory “normoxic” conditions of 18% oxygen.²³ Collectively, these data show a role for hypoxia to limit RSV infection and pharmacological activation of HIF in multiple cell lines and PBEC, demonstrating its role in restricting RSV infection.

Prolyl-hydroxylase inhibitors inhibit RSV replication kinetics

To investigate how HIFs regulate RSV replication, we used an RSV reporter system with GFP inserted as a separate transcription unit in the viral genome, allowing us to monitor viral replication kinetics. Calu-3 cells were pretreated with Daprodustat, Molidustat, or Roxadustat (50 μ M) for 24h before infecting with the recombinant RSV (MOI 0.2). All three drugs inhibit RSV replication, with Daprodustat showing the most potent activity and screening a range of drug concentrations showed an IC₅₀ of 9.0 μ M at 48hpi (Figures 2A and S5). Bovine RSV (bRSV) is genetically closely related to human RSV, and we observed a consistent inhibition of bRSV replication by all three drugs (Figure S6), highlighting a conserved interplay of the HIF signaling pathway across the orthopneumoviruses. We examined whether treating RSV infected Calu-3 cells (at 24 hpi or 48 hpi) with Daprodustat or Molidustat (50 μ M) could influence virus replication and noted a significant suppression under these conditions (Figure 2B). These data are consistent with a role for the PHIs to limit virus transmission. Importantly, pre-treating Calu-3 cells with Daprodustat (used at an IC₅₀ value of 9.0 μ M) and Palivizumab, a clinically approved RSV antibody,^{41,42} showed greater antiviral activity of the drug combination than either treatment alone (Figure 2C). These data show that PHIs limit the kinetics of human and bovine RSV replication and a combined treatment of Daprodustat and Palivizumab shows additive antiviral activity.

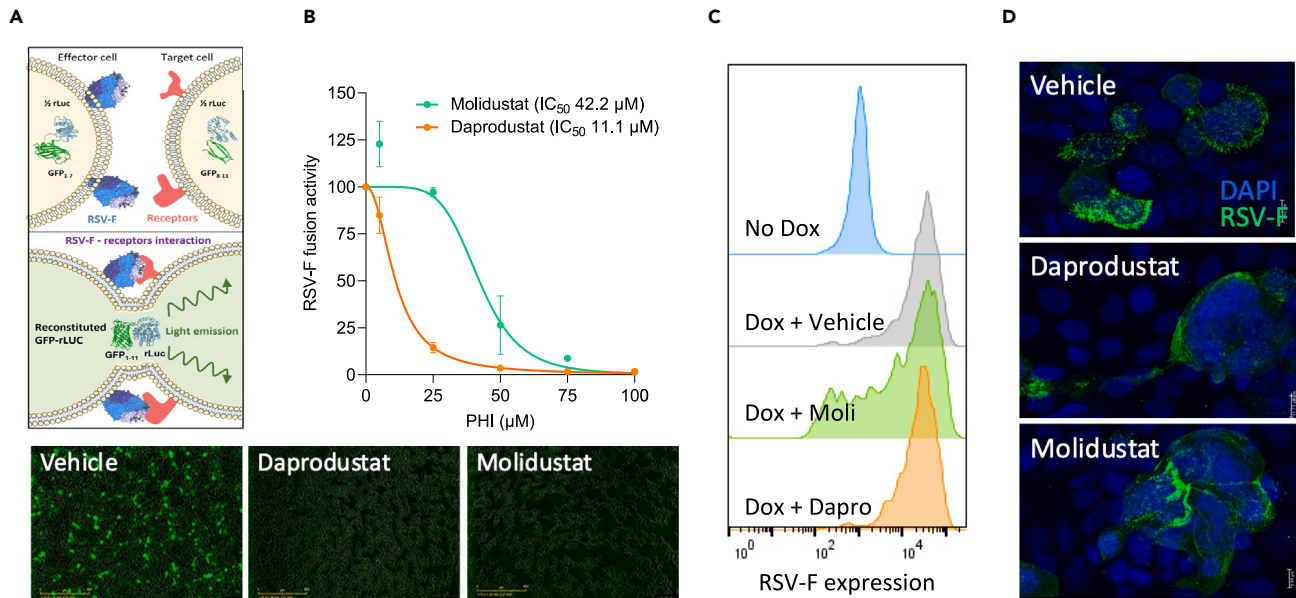


Figure 3. Inhibition of RSV-F mediated cell-cell fusion by prolyl-hydroxylase inhibitors

(A) HEK293T effector cells (expressing beta strands 1–7 of GFP), engineered to express a doxycycline-inducible RSV F protein, were cocultured with HEK293T target cells (expressing beta strands 8–11 of GFP).

(B) The inhibitory activity of Daprodustat or Molidustat was measured as GFP intensity signal 48h after co-culture (mean \pm SEM, n = 3).

(C) HEK293T cells were treated with PHI (50 μ M) in the presence of doxycycline and F expression analyzed by flow cytometry using an APC-conjugated anti-RSV-F antibody at 24hpi.

(D) Calu-3 cells were infected with RSV (MOI 1) and at 48hpi RSV-F expression imaged.

Inhibition of RSV-F mediated cell-cell fusion by prolyl-hydroxylase inhibitors

To elucidate the potential mechanism of action of the PHIs on the RSV life cycle, we examined RSV-F driven cell-cell fusion using a split GFP-luciferase reporter cell-cell fusion system, which uses a doxycycline inducible expression of RSV-F in an effector cell line, combined with a target cell line stably expressing the corresponding half of the reporter (Figure 3A).⁴³ Treatment with Daprodustat and Molidustat resulted in a dose-dependent inhibition of RSV-F cell-cell fusion with estimated IC_{50} values of 11 and 42 μ M, respectively (Figure 3B). To ensure that this activity was RSV-F dependent and not explained by the modulation of the split GFP-luciferase reporters, we co-transfected the constructs encoding the half reporters into cells and their activity was not affected by Daprodustat or Molidustat treatment (Figure S7). To investigate whether the PHIs interfere with RSV-F expression in the effector cells, we measured cell surface RSV-F expression by flow cytometry and treatment had a negligible effect (Figure 3C). Furthermore, immunofluorescence analysis indicated that none of the PHIs caused gross changes to the cellular distribution of RSV-F in infected Calu-3 cells (Figure 3D). Collectively, these data show that PHIs inhibit RSV-F driven cell-cell fusion.

Hypoxia and prolyl-hydroxylase inhibitors reduce nucleolin expression via regulating miR-494

We next investigated whether PHIs regulate the expression of the reported entry host factors for RSV: ICAM1,³² EGFR³³ and NCL³⁴ that may contribute to their anti-viral activity. Analysis of our earlier published transcriptomic data of hypoxic or Roxadustat treated Calu-3 cells²⁴ showed a significant reduction in NCL gene expression (Figure 4A). We validated our RNA-seq data and showed that NCL mRNA and protein expression were reduced in Calu-3 cells cultured under low oxygen conditions (1% oxygen) (Figure 4B). As a control we confirmed low oxygen induction of NDRG1 gene expression. Daprodustat treatment reduced NCL mRNA and protein expression as assessed by immunoblotting (Figure 4C) and flow cytometric analysis of Calu-3 and HEp-2 cells (Figures 4D and S8). As HIFs are well established transcription activators and generally considered positive regulators of gene expression,⁴⁴ we hypothesised this phenotype of reducing NCL expression is mediated by downstream HIF-signaling and potentially through the regulation of microRNAs. An earlier study reported that NCL transcripts were regulated by microRNA-494 (miR-494).⁴⁵ Notably, miR-494 has an HRE in its promoter (Figure S9) and was previously reported to be induced under hypoxic conditions.^{46,47} To examine this hypothesis, we measured miR-494 levels in Calu-3 cells cultured at 1% oxygen or treated with Daprodustat and found a robust induction (Figure 4E). Moreover, treatment with a miR-494 mimic reduced NCL protein expression and significantly reduced RSV infectivity (Figure 4F), supporting the HIF regulation of NCL expression through the induction of miR-494.

Daprodustat limits RSV infection and pulmonary inflammatory responses in mice

To assess the *in vivo* activity of Daprodustat, we administered the drug twice daily at a dose of 10 mg/kg or 30 mg/kg to mice and euthanised the animals after 4 days of treatment. This regimen was based on previous dosing protocols in mice.^{23,48} We confirmed the drug was

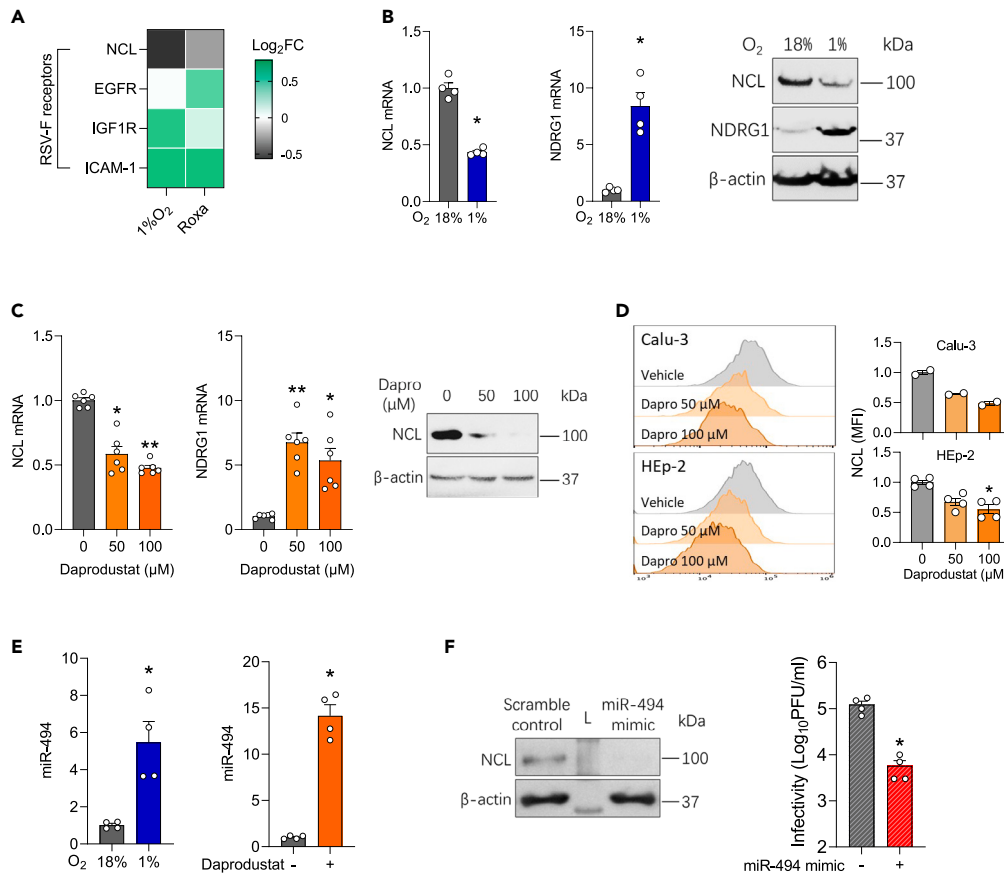


Figure 4. Hypoxia or prolyl-hydroxylase inhibitors inhibit nucleolin via regulating miR-494

(A) Calu-3 cells were cultured at 18% or 1% O₂ or treated with Roxadustat (50 μM) for 48h and cellular RNA sequenced. Differential expression analysis was performed to interrogate the expression of host entry factors that regulate RSV fusion, where the heatmap denotes Log₂ Fold change (FC).
(B) Calu-3 cells were cultured at 18% or 1% O₂ for 48h and NCL and NDRG1 mRNA or protein expression measured by qPCR or immunoblotting, respectively (mean ± SEM, n = 4, Mann-Whitney test, Two-sided).
(C) Calu-3 cells were treated with Daprodustat for 48h and NCL mRNA and protein expression determined by qPCR and immunoblotting, respectively (mean ± SEM, n = 6, One-way ANOVA with multiple comparisons, Two-sided).
(D) Calu-3 or HEP-2 cells were treated with Daprodustat for 48h and total NCL protein expression determined by flow cytometry (mean ± SEM, n = 2–4, One-way ANOVA with multiple comparisons, Two-sided).
(E) Calu-3 cells were cultured at 18% or 1% O₂ or treated with Daprodustat (50 μM) for 48h and miR-494 expression measured by qPCR (mean ± SEM, n = 4, Mann-Whitney test, Two-sided).
(F) Calu-3 cells were pre-treated with a miR-494 mimic (1 μM) for 24h before infecting with RSV (MOI 0.2) and intracellular infectivity determined at 48 hpi (mean ± SEM, n = 4, Mann-Whitney test, Two-sided). L = Molecular weight ladder. * denotes p < 0.05 and ** < 0.01.

well-tolerated as there was no evidence of weight loss or histopathological changes in the lungs (Figures 5A and S10). As HIF expression following systemic PHI treatment is transient and difficult to detect,⁴⁹ we evaluated Daprodustat efficacy by assessing the HIF activation of erythropoietin stimulated erythrocytosis by measuring immature red blood cells (reticulocytes). Blood smears from terminal blood samples showed increased reticulocyte counts compared to vehicle, consistent with effective drug treatment (Figure 5B). To establish whether oral delivery of Daprodustat was effective in the lower respiratory tract we showed activation of endothelin 1 (*Edn1*), a gene reported to be HIF regulated in the respiratory tract⁵⁰ (Figure 5B). In addition we observed reduced NCL gene expression in the lung of Daprodustat treated mice (Figure 5B).

To evaluate the anti-viral activity of Daprodustat, we infected mice intranasally with RSV and treated with the drug at 30 mg/kg using the same dosing schedule as above, followed by euthanasia at 4 dpi. We observed a minimal weight loss in the vehicle or Daprodustat treated RSV infected groups. We confirmed HIF pathway activation by measuring reticulocyte counts and increased *Edn1* expression in the Daprodustat treated group. We observed a reduction in *Ncl* mRNA and protein along with an increase in *miR-494* levels in the drug treated group compared to the vehicle controls (Figures 5C and 5D). In Daprodustat treated mice there was a significant reduction in the infectious RSV titer in the lung (Figure 5E). Immunohistological staining of the lungs for RSV antigen detected virus infected type I and II pneumocytes in low numbers of random disseminated alveoli, and with lower frequency in the drug treated mice (Figure 5F).

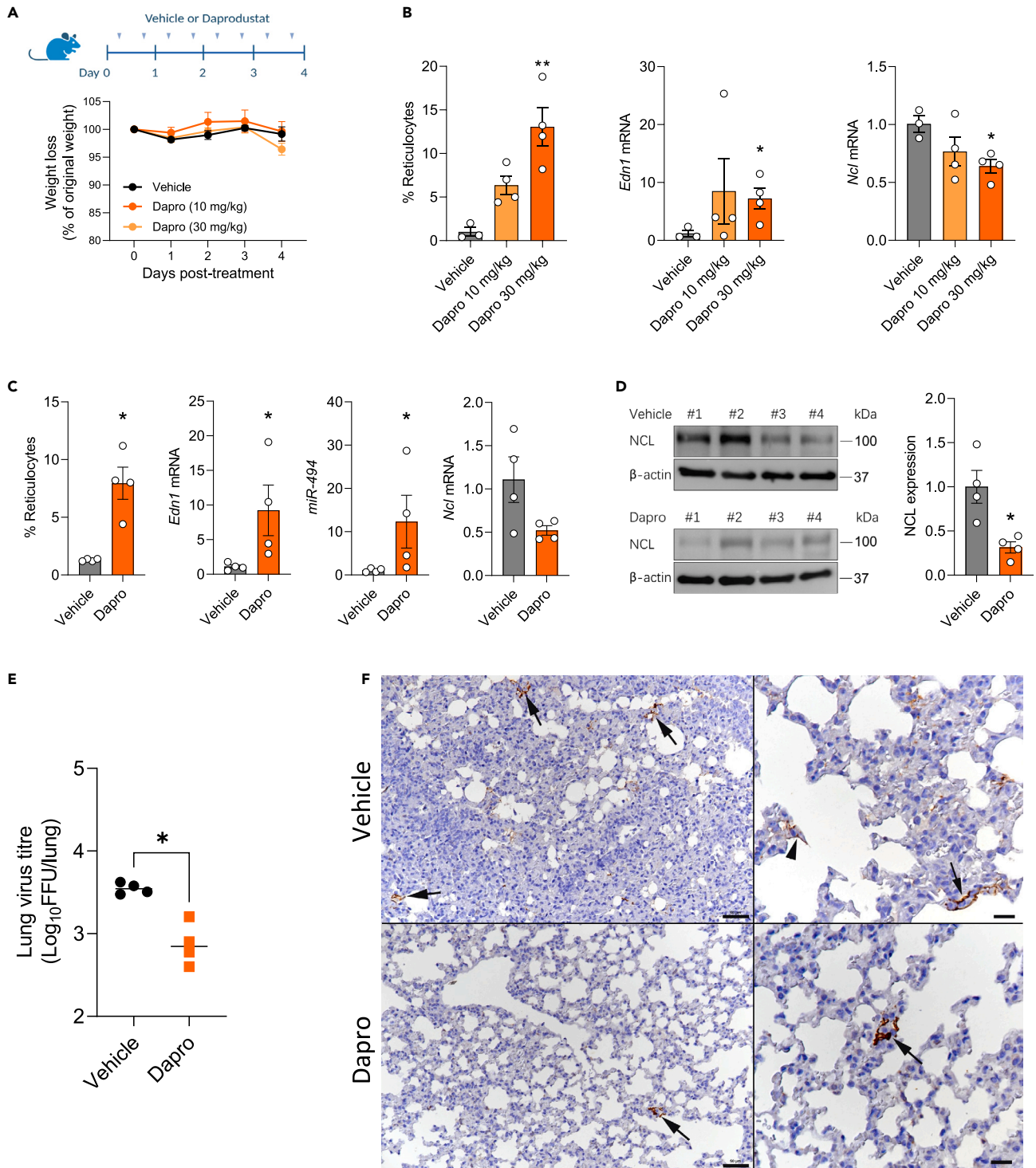


Figure 5. Daprodustat treatment reduces RSV infection in mice

(A) BALB/c mice (6–8 weeks old, female) were treated with vehicle (1% methylcellulose) or Daprodustat (10 or 30 mg/kg), twice daily via oral gavage for 4 days (B) Reticulocyte counts were measured and RNA extracted from the lung and *Edn1* and *Ncl* mRNA levels measured by qPCR (mean \pm SEM, vehicle $n = 3$; Daprodustat $n = 4$, One-way ANOVA with multiple comparisons, Two-sided). (C) BALB/c mice (6–8 weeks old, female) were treated with vehicle (1% methylcellulose) or Daprodustat (30 mg/kg), BID, via oral gavage 24h prior to intranasal infection with RSV A2 (1×10^7 PFU) and treated with drug as stated in (A) for 4 days. At the end of the experiment, reticulocyte counts were performed, and RNA extracted from the lung for the qPCR measurement of *Edn1*, *miR-494* and *Ncl* mRNA levels (mean \pm SEM, $n = 4$, Mann–Whitney test, Two-sided).

Figure 5. Continued

(D) Lung homogenates were assessed for NCL protein expression by immunoblotting and densitometric analysis quantified. NCL in individual samples were normalised to their β -actin loading controls (mean \pm SEM, n = 4, Mann–Whitney test, Two-sided).
(E) RSV infectivity in lung homogenate was measured by a focus forming assay (mean \pm SEM, n = 4, Mann–Whitney test, Two-sided).
(F) Representative images of lungs from mice at 4 dpi. The lung of a vehicle treated mouse exhibits several small patches of alveoli with RSV antigen positive pneumocytes (left: arrows). A higher magnification (right) shows infected type I pneumocytes (arrowhead) and type II pneumocytes (arrow). The lung of a Daprodustat (30 mg/kg) treated mouse shows a single patch of viral antigen expressing pneumocytes (left: arrow). The higher magnification of the patch (right; arrow) confirms that both type I and II pneumocytes are infected. Immunohistology, hematoxylin counterstain. Bars = 50 μ m (left) and 20 μ m (right).
* denotes $p < 0.05$ and ** < 0.01 .

RSV infection was accompanied by a generally mild inflammatory response, represented by mononuclear perivascular and/or peribronchial infiltrates (Figure 6). This was more extensive in the vehicle treated mice where it was accompanied by leukocyte rolling, subendothelial accumulation and infiltration of vascular walls (vasculitis), with circular perivascular accumulation in several layers. In Daprodustat treated mice, there was minimal leukocyte recruitment, with often fragmentary and thin perivascular accumulation. The dominant cells recruited from the vessels were monocytes (Iba1+) and T cells (CD3⁺), intermingled with rare neutrophils (Ly6G+). In addition, all lungs exhibited rare to a few small focal parenchymal areas with activated type II pneumocytes and infiltrating macrophages, lymphocytes and neutrophils (Figure 6).

RNA sequencing of the lung from vehicle or Daprodustat treated mice confirmed an activation of hypoxic-regulated pathways including glycolysis and showed evidence of increased interferon (alpha/gamma), TNF and TGFbeta signaling, consistent with an increase in immune signaling pathways (Figure S11). Cholesterol is an essential lipid in the life cycle of virtually all viruses,⁵¹ including RSV⁵² and it is notable that Daprodustat suppressed cholesterol homeostasis pathways (Figure S11). These transcriptomic analyses support a wide-ranging role for Daprodustat to perturb immune signaling pathways that will impact RSV replication and are worthy of further study. Together these data demonstrate that Daprodustat treatment reduced the frequency of RSV infected pneumocytes and infectious viral burden in treated mice.

DISCUSSION

The interplay between HIF-signalling pathways and human pathogens has been studied for multiple viruses⁵³ and more recently in the context of respiratory viral infections.^{23,24,54} RSV, Influenza and SARS-CoV-2 replicate within the respiratory tract, leading to cell damage and triggering an inflammatory response that disrupts oxygen distribution and contributes to local hypoxia. Influenza A virus infection of mice with HIF-1 α knock-out in type II alveolar epithelial cells²² showed a significant increase in viral replication, highlighting an antiviral role for HIF-1 α in this respiratory disease. The pathogen specific mechanisms and interactions with HIFs may vary depending on the virus, and understanding this relationship will underpin the development of effective treatments and interventions for respiratory viral infections.

Hypoxic conditions or treatment with PHIs to stabilise HIFs suppressed RSV replication. We confirmed this antiviral phenotype in Calu-3 and HEP-2 epithelial cell lines, in BEAS-2B that are derived from normal human bronchial epithelium and ALI PBEC cultures. RSV can induce robust syncytia formation *in vitro* and our real-time imaging showed that PHIs inhibit cell-cell fusion and spread of a GFP-expressing recombinant RSV. Moreover, the addition of Palivizumab further enhanced this inhibition. Through an RSV F protein-driven cell-cell fusion assay, we established that viral spread was a primary target of the PHIs (Daprodustat or Molidustat), and identified the downregulation of the RSV receptor nucleolin as the likely mechanism. We demonstrated the sensitivity of RSV to Daprodustat-mediated nucleolin knockdown *in vivo* using an experimental mouse model of RSV infection, and showed upregulation of the HIF-regulated microRNA - miR-494. Overall, these findings provide a mechanistic link between HIF-mediated transcription and inhibition of RSV infection. PHIs were developed as erythropoiesis-stimulating agents for treating anemic patients with chronic kidney disease. One limitation with repurposing this class of drugs is their primary pharmacological activity to increase hemoglobin concentrations.⁵⁵ However, there are several PHIs available with different selectivities⁵⁶ and evaluating their antiviral activity in an RSV mouse model would be worth investigating.

Earlier studies reported that RSV infection induced glycolysis via activating HIF-1 α expression and the HIF-1 α inhibitor PX-478 reduced virus replication.^{36,37,57} PX-478 has been reported to reduce HIF-1 α mRNA levels and translation under both normoxic and hypoxic conditions,⁵⁸ which may complicate the interpretation of these studies in assessing the effect(s) of HIF-signalling on the RSV life cycle. We did not observe HIF-1 α protein or activity in RSV infected Calu-3 cells and noted limited evidence of HIF regulated gene expression in the infected ALI-PBEC cultures. These differing results may reflect the variable proliferative and metabolic status of the infected target cells that can influence their glycolytic rate and endogenous HIF-signalling pathways. Recent reports demonstrate that RSV encoded matrix protein induces a perinuclear clustering of the mitochondria and infection perturbs mitochondrial function, resulting in increased reactive oxygen species (ROS).^{59,60} The impact of ROS on the transcriptional and translational regulation of HIF-1 α are complex and can activate different genes to those seen under hypoxia (reviewed in⁶¹). Hypoxic conditions have been reported to induce perinuclear clustering of mitochondria to create an oxidant-rich environment that is important for downstream gene regulation and HIF-signaling.^{62–65} Further investigations are warranted to better understand the interplay between RSV induced changes in cellular metabolism and HIF signaling pathways.

We demonstrate that miR-494 is induced under hypoxia and Daprodustat treatment. Moreover, we found that a miR-494 mimic reduced NCL expression and inhibited RSV infection, revealing an important role of oxygen-sensing microRNAs in regulating RSV infection. However, additional factors may influence NCL expression. The interaction between HIF and the transcriptional regulator c-myc may also suppress NCL expression. Myc regulates the transcription of NCL via binding e-boxes in the gene promoter,⁶⁶ however Myc requires MAX, its binding partner, to activate gene expression.⁶⁷ In hypoxic conditions, MAX is sequestered by HIF-1 α , which impairs its ability to transcribe target genes

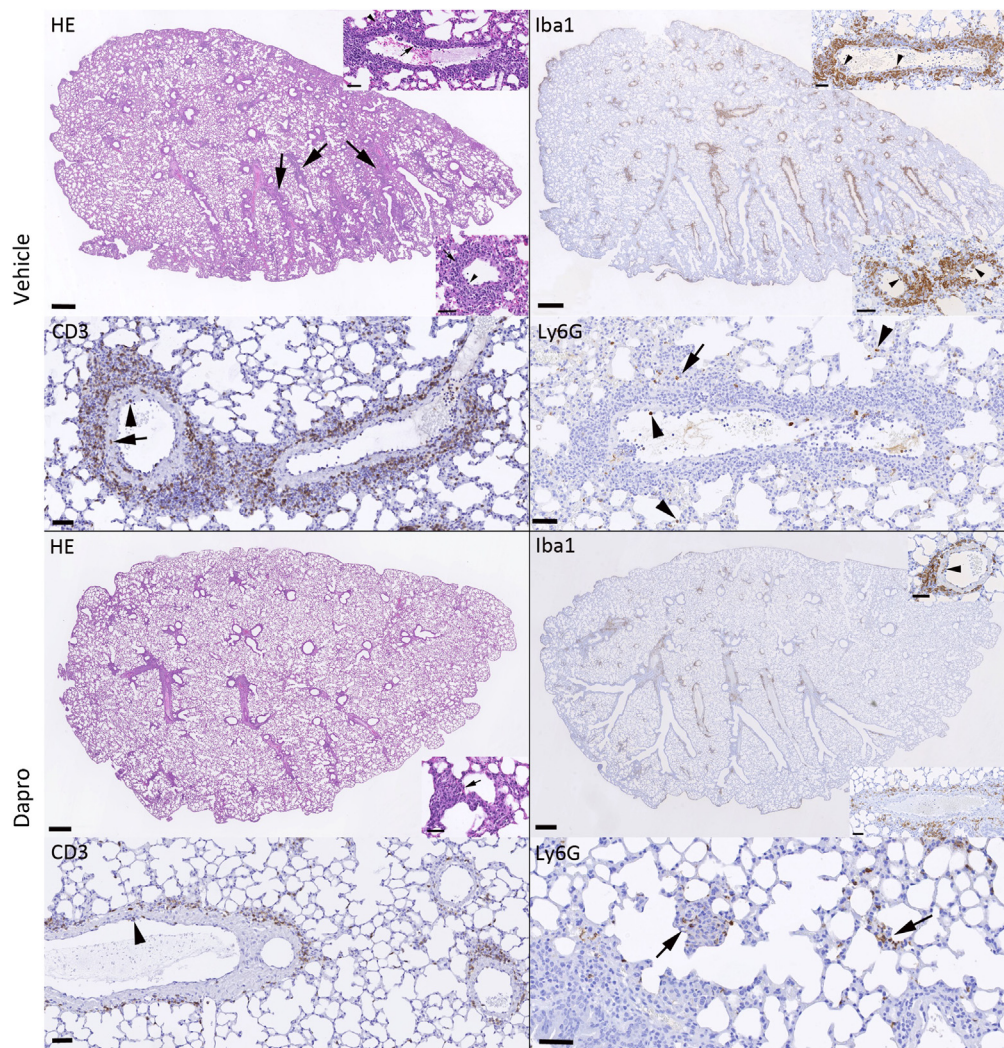


Figure 6. Daprodustat treatment reduces the RSV-associated pulmonary inflammatory responses in mice

Representative images of lungs from mice at 4 days post RSV infection. As shown in the HE stained section, the lung of a vehicle treated mouse exhibits mild perivascular and peribronchial mononuclear infiltrates (arrows) associated with leukocyte rolling and emigration (bottom inset, arrowhead) and subendothelial leukocyte aggregates in particular in muscular veins (top inset, arrowhead) consistent with vasculitis. The infiltrates are dominated by monocytes/macrophages (Iba1+) which are also found rolling and attached to the endothelium (bottom inset: arrowheads) and within the subendothelial infiltrates (top inset: arrowheads). T cells (CD3⁺) are numerous and present rolling (arrowhead) and within the vascular wall (arrow). There are a few neutrophils (Ly6G), within the lumen of vessels and capillaries (arrowheads) and occasionally within the small parenchymal infiltrates (arrow). After Daprodustat treatment, the inflammatory response is limited to very mild perivascular mononuclear infiltrates and rare small focal parenchymal infiltrates (HE stain: inset, arrow). The infiltrate shows a similar composition as in the vehicle treated mice. It is dominated by monocytes/macrophages (Iba1+) that are occasionally found also in vascular walls (top inset: arrowhead), followed by T cells (CD3⁺) that are occasionally seen rolling along the vascular endothelium (arrowhead). Neutrophils (Ly6G+) are mainly seen in the rare small parenchymal infiltrates (arrows). Bars = 500 μ m (whole section images) and 50 μ m (all other images).

including NCL. RNA-seq analysis of the lung from vehicle or Daprodustat treated mice showed an enrichment in Myc target pathways (Figure S11). It is likely that other oxygen sensitive pathways, such as chromatin conformation and DNA methylation may further modulate NCL expression in hypoxic conditions. NCL was reported to interact with Influenza virus non-structural protein 1 and to regulate late viral gene expression,^{68,69} and to also mediate SARS-CoV-2 replication,⁷⁰ suggesting a wide-ranging impact for the hypoxic regulation of NCL in respiratory infections.

Tayyari et al. identified NCL as a human RSV receptor using several experimental approaches including siRNA knockdown, antibody interference, overexpression in non-permissive cells and *in vivo* challenge studies.³⁴ We confirmed a role for NCL in RSV infection of Calu-3 cells by showing reduced infection following transient siRNA mediated knock-down of NCL expression (Figure S12). NCL ligands such as

pseudopeptide HB-199, midkine or pleiotrophin have been proposed as potential therapeutics against RSV.^{71–73} Mastrangelo et al. reported that the NCL binding anti-cancer drug, AS1411, could ameliorate RSV infection.⁷⁴ More recently, the same authors reported that RSV-F binds the RNA binding domains 1 and 2 of NCL and peptides from this region could inhibit RSV infection.⁷⁵ As NCL has been reported to interact with other viruses including parainfluenza type 3,⁷⁶ enterovirus 71,⁷⁷ Crimean–Congo haemorrhagic fever virus⁷⁸ and adeno-associated virus type 2,⁷⁹ our observation showing the HIF/miR494 regulation of NCL may be widely applicable to many viruses.

NCL is often over-expressed in cancer cells and although the mechanisms for its cell surface expression are not well characterised, NCL is thought to cluster at the membrane through cytoskeletal interactions.⁸⁰ Deregulation and over-expression of NCL on the cell surface have been associated with lower survival rates, potentially defining it as a biomarker. Moreover, the ability of NCL to internalise a range of ligands in a calcium-dependent manner has made it an attractive target for therapeutic intervention (reviewed in⁸¹). It is intriguing to speculate that hypoxic conditions or pharmacological stabilization of HIFs, as modeled in our study, may disrupt cancer-specific surface NCL overexpression. Nucleolin is widely targeted for intracellular drug delivery, and this newly identified mechanism for its downregulation may shed further light on the role of this protein in cancer development, particularly considering the hypoxic nature of many solid tumors. It is worth noting that while the majority of our work was performed in Calu-3 cells, a non-small-cell lung cancer line, we observed similar phenotypes in BEAS-2B cells and in ALI-PBEC which are derived from normal bronchial epithelium.

Using an established RSV mouse model we show that Daprodustat treatment reduced the level of infectious virus and this was accompanied by a reduced frequency of RSV antigen expressing pneumocytes. The frequency of infected cells in the lung at 4dpi was low and this may reflect the semi-permissive nature of hRSV infection of mice (reviewed in⁸²). Despite the low frequency of infection, RSV induced a similar inflammatory response as seen with other respiratory viruses, such as SARS-CoV-2 and IAV, with clear evidence of leukocyte recruitment and monocyte and T cell driven vasculitis and perivascular/peribronchial infiltration.⁸³ Daprodustat treatment dampened these inflammatory responses, although the recruitment of neutrophils was maintained, in line with earlier reports on hypoxia driving neutrophilic inflammation.⁸⁴ Preliminary experiments in mice infected with the genetically related pneumovirus of mice (PVM), a natural pathogen of rodents, support our findings with hRSV and showed a reduced frequency of infected cells and a less intense inflammatory response following Daprodustat treatment. Further studies are warranted to identify the inflammatory cells and their localisation with RSV infected epithelial cells during the acute and resolution phases of disease. Reassuringly, these observations align with our recent report that treating hamsters with the PHI Roxadustat reduced SARS-CoV-2 infection and epithelial damage,²⁴ highlighting a conserved role for HIFs to suppress respiratory viruses.

In summary, our study has uncovered an important mechanism for HIF to downregulate NCL, the cell surface receptor for RSV, that is mediated through the transcriptional activation of miR-494. Whilst our findings support a role for HIFs to limit RSV RNA replication understanding the detailed molecular mechanisms is beyond the remit of the current study. A recent report that hypoxia promotes JMJD6 mediated hydroxylation of proteins in regions predicted to be unstructured and associated with membraneless organelle formation⁸⁵ provides a potential mechanism for HIF-independent hypoxic pathways to perturb RSV RNA replication and is worthy of investigation. This study highlights a role for HIF-signalling to limit multiple aspects of RSV infection and associated inflammatory responses.

Limitations of the study

One limitation of our study is the single time-point of sampling the infected mice and additional kinetic studies to assess the effect of PHIs on RSV infection dynamics and immune infiltration are warranted. Given the limited frequency of RSV-infected epithelia in the mouse lung we were unable to assess whether HIFs perturbed the pattern of viral RNAs using direct-RNA sequencing approaches and single-cell *in situ* sequencing approaches would offer invaluable insights.

STAR★METHODS

Detailed methods are provided in the online version of this paper and include the following:

- KEY RESOURCES TABLE
- RESOURCE AVAILABILITY
 - Lead contact
 - Materials availability
 - Data and code availability
- EXPERIMENTAL MODEL AND STUDY PARTICIPANT DETAILS
 - Cell lines and primary cells
- METHOD DETAILS
 - Reagents
 - RNA-sequencing analysis
- QUANTIFICATION AND STATISTICAL ANALYSIS

SUPPLEMENTAL INFORMATION

Supplemental information can be found online at <https://doi.org/10.1016/j.isci.2023.108763>.

ACKNOWLEDGMENTS

The authors are grateful to the laboratory technicians, Histology Laboratory, Institute of Veterinary Pathology, Vetsuisse Faculty, University of Zurich, for excellent technical support. We acknowledge the support of Geraldine Taylor (The Pirbright Institute), Ursula Buchholz (NIAID, NIH) and Karl-Klaus Conzelmann (Max-von-Pettenkofer Institut) for providing recombinant viruses, Tim Hinks (Oxford University, UK) for human PBECs, Julian Hiscox (University of Liverpool) for sharing RSV minigenome reagents and Nadina Wand for critical reading of the article. The McKeating laboratory is funded by a Wellcome Investigator Award (IA) 200838/Z/16/Z, UK Medical Research Council (MRC) project grant MR/R022011/1 and Chinese Academy of Medical Sciences (CAMS) Innovation Fund for Medical Science (CIFMS), China (grant number: 2018-I2M-2-002). HB is funded by Wellcome Trust Studentship 108869/Z/15/Z. The Stewart laboratory is supported by UK Medical Research Council (MRC) grants MR/W021641/1, MR/W005611/1, Innovate UK grant TS/W022648/1, Biotechnology and Biological Sciences Research Council grant BB/W020351/1 and Wellcome Trust grant 223733/Z/21/Z. DB and GG acknowledge the Pirbright Institute flow cytometry facility and were supported by MRC (MR/P021735/1) and BBSRC grants (BB/W006162/1) and BBSRC Institute Strategic Program Grant (ISPG) to the Pirbright Institute (BBS/E/I/00007034, BBS/E/I/00007039, BBS/E/I/00007037, BBS/E/I/00007038 and BBS/E/I/00007030). The funders had no role in study design, data collection and analysis, decision to publish, or preparation of the article.

AUTHOR CONTRIBUTIONS

XZ, DB, and JAM conceived the project; XZ, GG, PS, AM, HB, JMH, ST, PB, JS, DB, and JAM designed experiments; XZ, GG, PS, AM, HB, JMH, JH, EB, AK, SN, DM, and PB generated data; XZ, GG, PS, AM, HB, JMH, JH, PB, DM, AK, JS, DB, and JAM analyzed and interpreted data; ST, HY, and PACW provided essential reagents and expertise; XZ and JAM prepared the article. All authors provided critical review of the article.

DECLARATION OF INTERESTS

None of the authors have any competing interests to declare.

Received: August 18, 2023

Revised: October 13, 2023

Accepted: December 15, 2023

Published: December 18, 2023

REFERENCES

- Shi, T., McAllister, D.A., O'Brien, K.L., Simoes, E.A.F., Madhi, S.A., Gessner, B.D., Polack, F.P., Balsells, E., Acacio, S., Aguayo, C., et al. (2017). Global, regional, and national disease burden estimates of acute lower respiratory infections due to respiratory syncytial virus in young children in 2015: a systematic review and modelling study. *Lancet* 390, 946–958.
- Fleming, D.M., Taylor, R.J., Lustig, R.L., Schuck-Paim, C., Haguin, F., Webb, D.J., Logie, J., Matias, G., and Taylor, S. (2015). Modelling estimates of the burden of Respiratory Syncytial virus infection in adults and the elderly in the United Kingdom. *BMC Infect. Dis.* 15, 443.
- Grayson, S.A., Griffiths, P.S., Perez, M.K., and Piedimonte, G. (2017). Detection of airborne respiratory syncytial virus in a pediatric acute care clinic. *Pediatr. Pulmonol.* 52, 684–688.
- Collins, P.L., and Graham, B.S. (2008). Viral and host factors in human respiratory syncytial virus pathogenesis. *J. Virol.* 82, 2040–2055.
- Homaira, N., Rawlinson, W., Snelling, T.L., and Jaffe, A. (2014). Effectiveness of Palivizumab in Preventing RSV Hospitalization in High Risk Children: A Real-World Perspective. *Int. J. Pediatr.* 2014, 571609.
- Kingwell, K. (2023). RSV vaccines score landmark FDA approvals. *Nat. Rev. Drug Discov.* 22, 523–525.
- Peebles, R.S., Jr., and Graham, B.S. (2005). Pathogenesis of respiratory syncytial virus infection in the murine model. *Proc. Am. Thorac. Soc.* 2, 110–115.
- Reichert, H., Suh, M., Jiang, X., Movva, N., Bylsma, L.C., Fryzek, J.P., and Nelson, C.B. (2022). Mortality Associated With Respiratory Syncytial Virus, Bronchiolitis, and Influenza Among Infants in the United States: A Birth Cohort Study From 1999 to 2018. *J. Infect. Dis.* 226, S246–S254.
- Bylsma, L.C., Suh, M., Movva, N., Fryzek, J.P., and Nelson, C.B. (2022). Mortality Among US Infants and Children Under 5 Years of Age with Respiratory Syncytial Virus and Bronchiolitis: A Systematic Literature Review. *J. Infect. Dis.* 226, S267–S281.
- Corcoran, S.E., and O'Neill, L.A.J. (2016). HIF1alpha and metabolic reprogramming in inflammation. *J. Clin. Invest.* 126, 3699–3707.
- Kaelin, W.G., Jr., and Ratcliffe, P.J. (2008). Oxygen sensing by metazoans: the central role of the HIF hydroxylase pathway. *Mol. Cell* 30, 393–402.
- Palazon, A., Goldrath, A.W., Nizet, V., and Johnson, R.S. (2014). HIF transcription factors, inflammation, and immunity. *Immunity* 41, 518–528.
- Urrutia, A.A., and Aragonés, J. (2018). HIF Oxygen Sensing Pathways in Lung Biology. *Biomedicines* 6, 68.
- Watts, E.R., and Walmsley, S.R. (2019). Inflammation and Hypoxia: HIF and PHD Isoform Selectivity. *Trends Mol. Med.* 25, 33–46.
- Huang, X., Zhang, X., Zhao, D.X., Yin, J., Hu, G., Evans, C.E., and Zhao, Y.Y. (2019). Endothelial Hypoxia-Inducible Factor-1alpha Is Required for Vascular Repair and Resolution of Inflammatory Lung Injury through Forkhead Box Protein M1. *Am. J. Pathol.* 189, 1664–1679.
- Polke, M., Seiler, F., Lepper, P.M., Kamyschnikow, A., Langer, F., Monz, D., Herr, C., Bals, R., and Beisswenger, C. (2017). Hypoxia and the hypoxia-regulated transcription factor HIF-1alpha suppress the host defence of airway epithelial cells. *Innate Immun.* 23, 373–380.
- McClendon, J., Jansing, N.L., Redente, E.F., Gandjeva, A., Ito, Y., Colgan, S.P., Ahmad, A., Riches, D.W.H., Chapman, H.A., Mason, R.J., et al. (2017). Hypoxia-Inducible Factor 1alpha Signaling Promotes Repair of the Alveolar Epithelium after Acute Lung Injury. *Am. J. Pathol.* 187, 1772–1786.
- Tojo, K., Tamada, N., Nagamine, Y., Yazawa, T., Ota, S., and Goto, T. (2018). Enhancement of glycolysis by inhibition of oxygen-sensing prolyl hydroxylases protects alveolar epithelial cells from acute lung injury. *FASEB J.* 32, 2258–2268.
- Vohwinkel, C.U., Burns, N., Coit, E., Yuan, X., Vlahar, E.K., Sul, C., Schmidt, E.P., Carmeliet, P., Stenmark, K., Nozik, E.S., et al. (2022). HIF1A-dependent induction of alveolar epithelial PFKFB3 dampens acute lung injury. *JCI Insight* 7, e157855.
- Eckle, T., Brodsky, K., Bonney, M., Packard, T., Han, J., Borchers, C.H., Mariani, T.J., Kominsky, D.J., Mittelbronn, M., and Eltzschig, H.K. (2013). HIF1A reduces acute lung injury by optimizing carbohydrate metabolism in the alveolar epithelium. *PLoS Biol.* 11, e1001665.
- Vohwinkel, C.U., Coit, E.J., Burns, N., Elajaili, H., Hernandez-Saavedra, D., Yuan, X., Eckle,

- T., Nozik, E., Tuder, R.M., and Eltzschig, H.K. (2021). Targeting alveolar-specific succinate dehydrogenase A attenuates pulmonary inflammation during acute lung injury. *FASEB J.* 35, e21468.
22. Zhao, C., Chen, J., Cheng, L., Xu, K., Yang, Y., and Su, X. (2020). Deficiency of HIF-1 α enhances influenza A virus replication by promoting autophagy in alveolar type II epithelial cells. *Emerg. Microbes Infect.* 9, 691–706.
23. Wing, P.A.C., Keeley, T.P., Zhuang, X., Lee, J.Y., Prange-Barczynska, M., Tsukuda, S., Morgan, S.B., Harding, A.C., Argles, I.L.A., Kurlekar, S., et al. (2021). Hypoxic and pharmacological activation of HIF inhibits SARS-CoV-2 infection of lung epithelial cells. *Cell Rep.* 35, 109020.
24. Wing, P.A.C., Prange-Barczynska, M., Cross, A., Crotta, S., Orbegozo Rubio, C., Cheng, X., Harris, J.M., Zhuang, X., Johnson, R.L., Ryan, K.A., et al. (2022). Hypoxia inducible factors regulate infectious SARS-CoV-2, epithelial damage and respiratory symptoms in a hamster COVID-19 model. *PLoS Pathog.* 18, e1010807.
25. Chen, N., Hao, C., Liu, B.C., Lin, H., Wang, C., Xing, C., Liang, X., Jiang, G., Liu, Z., Li, X., et al. (2019). Roxadustat Treatment for Anemia in Patients Undergoing Long-Term Dialysis. *N. Engl. J. Med.* 381, 1011–1022.
26. Chen, N., Hao, C., Peng, X., Lin, H., Yin, A., Hao, L., Tao, Y., Liang, X., Liu, Z., Xing, C., et al. (2019). Roxadustat for Anemia in Patients with Kidney Disease Not Receiving Dialysis. *N. Engl. J. Med.* 381, 1001–1010.
27. Akizawa, T., Yamaguchi, Y., Otsuka, T., and Reusch, M. (2020). A Phase 3, Multicenter, Randomized, Two-Arm, Open-Label Study of Intermittent Oral Dosing of Roxadustat for the Treatment of Anemia in Japanese Erythropoiesis-Stimulating Agent-Naive Chronic Kidney Disease Patients Not on Dialysis. *Nephron* 144, 372–382.
28. Akizawa, T., Iwasaki, M., Yamaguchi, Y., Majikawa, Y., and Reusch, M. (2020). Phase 3, Randomized, Double-Blind, Active-Comparator (Darbepoetin Alfa) Study of Oral Roxadustat in CKD Patients with Anemia on Hemodialysis in Japan. *J. Am. Soc. Nephrol.* 31, 1628–1639.
29. Akizawa, T., Otsuka, T., Reusch, M., and Ueno, M. (2020). Intermittent Oral Dosing of Roxadustat in Peritoneal Dialysis Chronic Kidney Disease Patients with Anemia: A Randomized, Phase 3, Multicenter, Open-Label Study. *Ther. Apher. Dial.* 24, 115–125.
30. Akizawa, T., Nangaku, M., Yonekawa, T., Okuda, N., Kawamatsu, S., Onoue, T., Endo, Y., Hara, K., and Kobitz, A.R. (2020). Efficacy and Safety of Daprodustat Compared with Darbepoetin Alfa in Japanese Hemodialysis Patients with Anemia: A Randomized, Double-Blind, Phase 3 Trial. *Clin. J. Am. Soc. Nephrol.* 15, 1155–1165.
31. Battles, M.B., and McLellan, J.S. (2019). Respiratory syncytial virus entry and how to block it. *Nat. Rev. Microbiol.* 17, 233–245.
32. Behera, A.K., Matsuse, H., Kumar, M., Kong, X., Lockey, R.F., and Mohapatra, S.S. (2001). Blocking intercellular adhesion molecule-1 on human epithelial cells decreases respiratory syncytial virus infection. *Biochem. Biophys. Res. Commun.* 280, 188–195.
33. Currier, M.G., Lee, S., Stobart, C.C., Hotard, A.L., Villenave, R., Meng, J., Pretto, C.D., Shields, M.D., Nguyen, M.T., Todd, S.O., et al. (2016). EGFR Interacts with the Fusion Protein of Respiratory Syncytial Virus Strain 2-20 and Mediates Infection and Mucin Expression. *PLoS Pathog.* 12, e1005622.
34. Tayyari, F., Marchant, D., Moraes, T.J., Duan, W., Mastrangelo, P., and Hegele, R.G. (2011). Identification of nucleolin as a cellular receptor for human respiratory syncytial virus. *Nat. Med.* 17, 1132–1135.
35. Kilani, M.M., Mohammed, K.A., Nasreen, N., Tepper, R.S., and Antony, V.B. (2004). RSV causes HIF-1 α stabilization via NO release in primary bronchial epithelial cells. *Inflammation* 28, 245–251.
36. Haeberle, H.A., Dürrstein, C., Rosenberger, P., Hosakote, Y.M., Kuhlcke, J., Kempf, V.A.J., Garofalo, R.P., and Eltzschig, H.K. (2008). Oxygen-independent stabilization of hypoxia inducible factor (HIF)-1 during RSV infection. *PLoS One* 3, e3352.
37. Chen, L.F., Cai, J.X., Zhang, J.J., Tang, Y.J., Chen, J.Y., Xiong, S., Li, Y.L., Zhang, H., Liu, Z., and Li, M.M. (2023). Respiratory syncytial virus co-opts hypoxia-inducible factor-1 α -mediated glycolysis to favor the production of infectious virus. *mBio* 14, e0211023.
38. Tran, T.L., Castagné, N., Duboscq, V., Noiville, S., Koch, E., Moudjou, M., Henry, C., Bernard, J., Yeo, R.P., and Eléouët, J.F. (2009). The respiratory syncytial virus M2-1 protein forms tetramers and interacts with RNA and P in a competitive manner. *J. Virol.* 83, 6363–6374.
39. Rincheval, V., Lelek, M., Gault, E., Bouillier, C., Sitterlin, D., Blouquit-Laye, S., Galloux, M., Zimmer, C., Eleouet, J.F., and Rameix-Welti, M.A. (2017). Functional organization of cytoplasmic inclusion bodies in cells infected by respiratory syncytial virus. *Nat. Commun.* 8, 563.
40. Jorquera, P.A., Anderson, L., and Tripp, R.A. (2016). Human Respiratory Syncytial Virus: An Introduction. *Methods Mol. Biol.* 1442, 1–12.
41. Schmidt, R., Majer, I., García Román, N., Rivas Bastera, A., Grubb, E., and Medrano López, C. (2017). Palivizumab in the prevention of severe respiratory syncytial virus infection in children with congenital heart disease: a novel cost-utility modeling study reflecting evidence-based clinical pathways in Spain. *Health Econ. Rev.* 7, 47.
42. Rogovik, A.L., Carleton, B., Solimano, A., and Goldman, R.D. (2019). Palivizumab for the prevention of respiratory syncytial virus infection. *Can. Fam. Physician* 56, 769–772.
43. Thakur, N., Conceicao, C., Isaacs, A., Human, S., Modhiran, N., McLean, R.K., Pedrera, M., Tan, T.K., Rijal, P., Townsend, A., et al. (2021). Micro-fusion inhibition tests: quantifying antibody neutralization of virus-mediated cell-cell fusion. *J. Gen. Virol.* 102, jgv001506.
44. Smythies, J.A., Sun, M., Masson, N., Salama, R., Simpson, P.D., Murray, E., Neumann, V., Cockman, M.E., Choudhry, H., Ratcliffe, P.J., and Mole, D.R. (2019). Inherent DNA-binding specificities of the HIF-1 α and HIF-2 α transcription factors in chromatin. *EMBO Rep.* 20, e46401.
45. Tominaga, K., Srikantan, S., Lee, E.K., Subaran, S.S., Martindale, J.L., Abdelmohsen, K., and Gorospe, M. (2011). Competitive regulation of nucleolin expression by HuR and miR-494. *Mol. Cell Biol.* 31, 4219–4231.
46. Koehler, J., Sandey, M., Prasad, N., Levy, S.A., and Wang, X. (2020). Differential Expression of miRNAs in Hypoxia ("HypoxamiRs") in Three Canine High-Grade Glioma Cell Lines. *Front. Vet. Sci.* 7, 104.
47. Sun, G., Zhou, Y., Li, H., Guo, Y., Shan, J., Xia, M., Li, Y., Li, S., Long, D., and Feng, L. (2013). Over-expression of microRNA-494 up-regulates hypoxia-inducible factor-1 α expression via PI3K/Akt pathway and protects against hypoxia-induced apoptosis. *J. Biomed. Sci.* 20, 100.
48. Schley, G., Klanke, B., Kalucka, J., Schatz, V., Daniel, C., Mayer, M., Goppelt-Strube, M., Herrmann, M., Thorsteinsdottir, M., Palsson, R., et al. (2019). Mononuclear phagocytes orchestrate prolyl hydroxylase inhibition-mediated renoprotection in chronic tubulointerstitial nephritis. *Kidney Int.* 96, 378–396.
49. Chan, M.C., Iltot, N.E., Schödel, J., Sims, D., Tumber, A., Lippl, K., Mole, D.R., Pugh, C.W., Ratcliffe, P.J., Ponting, C.P., and Schofield, C.J. (2016). Tuning the Transcriptional Response to Hypoxia by Inhibiting Hypoxia-inducible Factor (HIF) Prolyl and Asparaginyl Hydroxylases. *J. Biol. Chem.* 291, 20661–20673.
50. Hickey, M.M., Richardson, T., Wang, T., Mosqueira, M., Argüiri, E., Yu, H., Yu, Q.C., Solomides, C.C., Morrissey, E.E., Khurana, T.S., et al. (2010). The von Hippel-Lindau Chuvash mutation promotes pulmonary hypertension and fibrosis in mice. *J. Clin. Invest.* 120, 827–839.
51. Glitscher, M., and Hildt, E. (2021). Endosomal Cholesterol in Viral Infections - A Common Denominator? *Front. Physiol.* 12, 750544.
52. San-Juan-Vergara, H., Sampayo-Escobar, V., Reyes, N., Cha, B., Pacheco-Lugo, L., Wong, T., Peoples, M.E., Collins, P.L., Castaño, M.E., and Mohapatra, S.S. (2012). Cholesterol-rich microdomains as docking platforms for respiratory syncytial virus in normal human bronchial epithelial cells. *J. Virol.* 86, 1832–1843.
53. Liu, P.J., Balfe, P., McKeating, J.A., and Schilling, M. (2020). Oxygen Sensing and Viral Replication: Implications for Tropism and Pathogenesis. *Viruses* 12.
54. Guo, X., Zhu, Z., Zhang, W., Meng, X., Zhu, Y., Han, P., Zhou, X., Hu, Y., and Wang, R. (2017). Nuclear translocation of HIF-1 α induced by influenza A (H1N1) infection is critical to the production of proinflammatory cytokines. *Emerg. Microbes Infect.* 6, e39.
55. Yeh, T.L., Leissing, T.M., Abboud, M.I., Thinnies, C.C., Atasoylu, O., Holt-Martyn, J.P., Zhang, D., Tumber, A., Lippl, K., Lohans, C.T., et al. (2017). Molecular and cellular mechanisms of HIF prolyl hydroxylase inhibitors in clinical trials. *Chem. Sci.* 8, 7651–7668.
56. Sulser, P., Pickel, C., Günter, J., Leissing, T.M., Crean, D., Schofield, C.J., Wenger, R.H., and Scholz, C.C. (2020). HIF hydroxylase inhibitors decrease cellular oxygen consumption depending on their selectivity. *FASEB J.* 34, 2344–2358.
57. Morris, D.R., Qu, Y., Agrawal, A., Garofalo, R.P., and Casola, A. (2020). HIF-1 α Modulates Core Metabolism and Virus Replication in Primary Airway Epithelial Cells Infected with Respiratory Syncytial Virus. *Viruses* 12.
58. Koh, M.Y., Spivak-Kroizman, T., Venturini, S., Welsh, S., Williams, R.R., Kirkpatrick, D.L., and Powis, G. (2008). Molecular mechanisms for the activity of PX-478, an antitumor inhibitor of the hypoxia-inducible factor-1 α . *Mol. Cancer Ther.* 7, 90–100.
59. Hu, M., Bogoyevitch, M.A., and Jans, D.A. (2023). Respiratory Syncytial Virus Matrix Protein Is Sufficient and Necessary to Remodel Host Mitochondria in Infection. *Cells* 12.

60. Hu, M., Schulze, K.E., Ghildyal, R., Henstridge, D.C., Kolanowski, J.L., New, E.J., Hong, Y., Hsu, A.C., Hansbro, P.M., Wark, P.A., et al. (2019). Respiratory syncytial virus co-opts host mitochondrial function to favour infectious virus production. *Elife* 8, e42448.
61. Movafagh, S., Crook, S., and Vo, K. (2015). Regulation of hypoxia-inducible factor-1 α by reactive oxygen species: new developments in an old debate. *J. Cell. Biochem.* 116, 696–703.
62. Al-Mehdi, A.B., Pastukh, V.M., Swiger, B.M., Reed, D.J., Patel, M.R., Bardwell, G.C., Pastukh, V.V., Alexeyev, M.F., and Gillespie, M.N. (2012). Perinuclear mitochondrial clustering creates an oxidant-rich nuclear domain required for hypoxia-induced transcription. *Sci. Signal.* 5, ra47.
63. Mori, M.P., Penjweini, R., Ma, J., Alspaugh, G., Andreoni, A., Kim, Y.C., Wang, P.Y., Knutson, J.R., and Hwang, P.M. (2023). Mitochondrial respiration reduces exposure of the nucleus to oxygen. *J. Biol. Chem.* 299, 103018.
64. Thomas, L.W., Staples, O., Turmaine, M., and Ashcroft, M. (2017). CHCHD4 Regulates Intracellular Oxygenation and Perinuclear Distribution of Mitochondria. *Front. Oncol.* 7, 71.
65. Xin, Y., Zhao, L., and Peng, R. (2023). HIF-1 signaling: an emerging mechanism for mitochondrial dynamics. *J. Physiol. Biochem.* 79, 489–500.
66. Greasley, P.J., Bonnard, C., and Amati, B. (2000). Myc induces the nucleolin and BN51 genes: possible implications in ribosome biogenesis. *Nucleic Acids Res.* 28, 446–453.
67. Blackwood, E.M., and Eisenman, R.N. (1991). Max: a helix-loop-helix zipper protein that forms a sequence-specific DNA-binding complex with Myc. *Science* 251, 1211–1217.
68. Murayama, R., Harada, Y., Shibata, T., Kuroda, K., Hayakawa, S., Shimizu, K., and Tanaka, T. (2007). Influenza A virus non-structural protein 1 (NS1) interacts with cellular multifunctional protein nucleolin during infection. *Biochem. Biophys. Res. Commun.* 362, 880–885.
69. Kumar, D., Broor, S., and Rajala, M.S. (2016). Interaction of Host Nucleolin with Influenza A Virus Nucleoprotein in the Early Phase of Infection Limits the Late Viral Gene Expression. *PLoS One* 11, e0164146.
70. Merino, V.F., Yan, Y., Ordonez, A.A., Bullen, C.K., Lee, A., Saeki, H., Ray, K., Huang, T., Jain, S.K., and Pomper, M.G. (2023). Nucleolin mediates SARS-CoV-2 replication and viral-induced apoptosis of host cells. *Antivir. Res.* 211, 105550.
71. Nisole, S., Said, E.A., Mische, C., Prevost, M.C., Krust, B., Bouvet, P., Bianco, A., Briand, J.P., and Hovanessian, A.G. (2002). The anti-HIV pentameric pseudopeptide HB-19 binds the C-terminal end of nucleolin and prevents anchorage of virus particles in the plasma membrane of target cells. *J. Biol. Chem.* 277, 20877–20886.
72. Said, E.A., Krust, B., Nisole, S., Svab, J., Briand, J.P., and Hovanessian, A.G. (2002). The anti-HIV cytokine midline binds the cell surface-expressed nucleolin as a low affinity receptor. *J. Biol. Chem.* 277, 37492–37502.
73. Said, E.A., Courty, J., Svab, J., Delbè, J., Krust, B., and Hovanessian, A.G. (2005). Pleiotrophin inhibits HIV infection by binding the cell surface-expressed nucleolin. *FEBS J.* 272, 4646–4659.
74. Mastrangelo, P., Norris, M.J., Duan, W., Barrett, E.G., Moraes, T.J., and Hegele, R.G. (2017). Targeting Host Cell Surface Nucleolin for RSV Therapy: Challenges and Opportunities. *Vaccines (Basel)* 5.
75. Mastrangelo, P., Chin, A.A., Tan, S., Jeon, A.H., Ackerley, C.A., Siu, K.K., Lee, J.E., and Hegele, R.G. (2021). Identification of RSV Fusion Protein Interaction Domains on the Virus Receptor, Nucleolin. *Viruses* 13, 261.
76. Bose, S., Basu, M., and Banerjee, A.K. (2004). Role of nucleolin in human parainfluenza virus type 3 infection of human lung epithelial cells. *J. Virol.* 78, 8146–8158.
77. Su, P.Y., Wang, Y.F., Huang, S.W., Lo, Y.C., Wang, Y.H., Wu, S.R., Shieh, D.B., Chen, S.H., Wang, J.R., Lai, M.D., and Chang, C.F. (2015). Cell surface nucleolin facilitates enterovirus 71 binding and infection. *J. Virol.* 89, 4527–4538.
78. Xiao, X., Feng, Y., Zhu, Z., and Dimitrov, D.S. (2011). Identification of a putative Crimean-Congo hemorrhagic fever virus entry factor. *Biochem. Biophys. Res. Commun.* 411, 253–258.
79. Qiu, J., and Brown, K.E. (1999). A 110-kDa nuclear shuttle protein, nucleolin, specifically binds to adeno-associated virus type 2 (AAV-2) capsid. *Virology* 257, 373–382.
80. Hovanessian, A.G., Puvion-Dutilleul, F., Nisole, S., Svab, J., Perret, E., Deng, J.S., and Krust, B. (2000). The cell-surface-expressed nucleolin is associated with the actin cytoskeleton. *Exp. Cell Res.* 261, 312–328.
81. Romano, S., Fonseca, N., Simões, S., Gonçalves, J., and Moreira, J.N. (2019). Nucleolin-based targeting strategies for cancer therapy: from targeted drug delivery to cytotoxic ligands. *Drug Discov. Today* 24, 1985–2001.
82. Taylor, G. (2017). Animal models of respiratory syncytial virus infection. *Vaccine* 35, 469–480.
83. De Neck, S., Penrice-Randal, R., Clark, J.J., Sharma, P., Bentley, E.G., Kirby, A., Mega, D.F., Han, X., Owen, A., Hiscox, J.A., et al. (2023). The Stereotypic Response of the Pulmonary Vasculature to Respiratory Viral Infections: Findings in Mouse Models of SARS-CoV-2, Influenza A and Gammaherpesvirus Infections. *Viruses* 15.
84. Morrison, T., Watts, E.R., Sadiku, P., and Walmsley, S.R. (2023). The emerging role for metabolism in fueling neutrophilic inflammation. *Immunol. Rev.* 314, 427–441.
85. Cockman, M.E., Sugimoto, Y., Pegg, H.B., Masson, N., Salah, E., Tumber, A., Flynn, H.R., Kirkpatrick, J.M., Schofield, C.J., and Ratcliffe, P.J. (2022). Widespread hydroxylation of unstructured lysine-rich protein domains by JMJD6. *Proc. Natl. Acad. Sci. USA* 119, e2201483119.
86. Ishikawa, H., Meng, F., Kondo, N., Iwamoto, A., and Matsuda, Z. (2012). Generation of a dual-functional split-reporter protein for monitoring membrane fusion using self-associating split GFP. *Protein Eng. Des. Sel.* 25, 813–820.
87. Seehusen, F., Clark, J.J., Sharma, P., Bentley, E.G., Kirby, A., Subramaniam, K., Wunderlin-Giuliani, S., Hughes, G.L., Patterson, E.I., Michael, B.D., et al. (2022). Neuroinvasion and Neurotropism by SARS-CoV-2 Variants in the K18-hACE2 Mouse. *Viruses* 14.

STAR★METHODS

KEY RESOURCES TABLE

REAGENT or RESOURCE	SOURCE	IDENTIFIER
Antibodies		
Mouse anti-HIF-1 α	BD Transduction Laboratories	clone#610959
Rabbit anti-NDRG1	Cell signaling	clone#5196
Mouse anti- β -actin	Sigma	clone#A5441
Mouse anti-RSV-F antibody	Pirbright	Made in-house, PMID:1383403
APC-conjugated anti-RSV-F antibody	Pirbright	Same antibody, conjugated in-house
Goat anti-RSV (IHC)	Millipore	AB1128
Rabbit anti-NCL (WB)	Abcam	clone#22758
Rabbit anti-NCL (IF)	Abcam	ab129200
Rabbit anti-Goat IgG HRP	Abcam	ab6741
Goat anti-Mouse IgG HRP	DAKO	clone#P0447
Rabbit IgG HRP Linked Whole Ab	Cytiva	clone#NA934
Goat anti-Rabbit Alexa 488nm	Thermo Fisher	A11034
Rabbit anti-Iba1	WAKO Pure Chemical Industries, Ltd.	019-19741
Rabbit anti-CD3 (clone SP7)	Abcam	ab16669
Rat anti-Ly6G (clone 1A8)	BioLegend	127602
Rabbit anti-rat IgG	Jackson Immuno Research Laboratories	312-005-045
Rabbit anti-goat IgG (HRP)	Abcam	ab6741
Envision+System HRP Rabbit	Dako	K4003
OmniMap anti-rabbit HRP	Roche	05 269 679 001
Palivizumab	MedChemtronica AB	HY-P9944
Bacterial and virus strains		
Human RSV subtype A	Kind gift from Magdalena A. Krzyzaniak	A2 strain
RSV-GFP	Kind gift from Magdalena A. Krzyzaniak	A2 strain
Bovine RSV	Kind gift from Ursula J. Buchholz	A51908 strain
Biological samples		
Primary bronchial epithelial cells	NHS, Oxford	PBECs
Chemicals, peptides, and recombinant proteins		
Daprodustat (GSK:1278863)	MedChemExpress	HY-17608
Molidustat (Bay 853934)	MedChemExpress	HY-12654
Roxadustat (FG-4592)	MedChemExpress	HY-13426
Cyclopamine	Cambridge Bioscience Ltd	C9710
SuperSignal West Dura Extended Duration Substrate	Thermo Fisher	34076
Live Dead Fixible Aqua stain	Life Technologies	50-112-1526
Critical commercial assays		
CytoTox 96 Non-Radioactive Cytotoxicity Assay	Promega	G1780
qPCR BIO SyGreen Blue Mix	PCR Biosystems Ltd	PB20.17-20
Firefly Luciferase Assay kit	Promega	E1501

(Continued on next page)

Continued

REAGENT or RESOURCE	SOURCE	IDENTIFIER
Experimental models: Cell lines		
Calu-3	Kind Gift from Professor Nicole Zitzmann	N/A
HEK293T	ATCC	CRL-3216
HEp-2	Pirbright Cell Service Unit	N/A
BEAS-2B	Pirbright Cell Service Unit	N/A
MDBK	Pirbright Cell Service Unit	N/A
Experimental models: Organisms/strains		
Mouse: Wild-type BALB/c	Charles River	BALB/cAnNCrl
Oligonucleotides		
Gene	Forward 5' – 3'	Reverse 5' – 3'
hNCL	GCCTGTCAAAGAAGCACCTGGA	GAAAGCCGTAGTCGGTTCTGTG
hNDRG1	TTTGATGTCCAGGAGCAGGA	ATGCCGATGTCATGGTAGGT
hB2M	CTACACTGAATTCACCCCCACTG	ACCTCCATGATGCTGCTTACATG
mNcl	TGAGGGCAGAACAATCAGGCTG	GGTCTCTTCAGTGGTATCCTCAG
mEdn1	CTACTTCTGCCACCTGGACATC	CGCACTGACATCTAACTGCCTG
mB2m	ACAGTTCACCCGCCTCACATT	TAGAAAGACCAGTCCTTGCTGAAG
RSV-F	TAAGCAGCTCCGTTATCACATCTC	ATTGGATGCTGTACATTTAGTTTTGC
Human NCL silencer select	Thermo Fisher	4390824
Silencer™ Select Negative Control No. 1 siRNA	Thermo Fisher	4390844
hsa-miR-494-5p mirVana® miRNA mimic	Thermo Fisher	MC26467
Recombinant DNA		
HRE-GFP	Kind gift from Professor James Nathan	N/A
Software and algorithms		
Prism 9	GraphPad	www.graphpad.com
Deposited data		
PRJNA991760	BioProject	www.ncbi.nlm.nih.gov

RESOURCE AVAILABILITY

Lead contact

Further information and requests for resources and reagents should be directed to and will be fulfilled by the lead contact Jane A McKeating (jane.mckeating@ndm.ox.ac.uk).

Materials availability

This study did not generate new unique reagents.

Data and code availability

- RNA-seq data from Daprodustat treated mice are deposited and can be accessible through NCBI (<https://www.ncbi.nlm.nih.gov>) as BioProject PRJNA991760.
- This paper does not report original code.
- Any additional information required to reanalyse the data reported in this paper is available from the [lead contact](#) upon request.

EXPERIMENTAL MODEL AND STUDY PARTICIPANT DETAILS

Cell lines and primary cells

All cells, including co-cultures, were cultured at 37°C and 5% CO₂ in a standard culture incubator and exposed to hypoxia using an atmosphere-regulated workstation set to 37°C, 5% CO₂ and 1% O₂ (InVivo 400, Baker-Ruskin Technologies). Calu-3 cells were cultured in Advanced DMEM (Sigma-Aldrich) supplemented with 10% fetal bovine serum (FBS), 2mM L-glutamine, 100 U/mL penicillin and 10 mg/mL

streptomycin (Invitrogen). HEp-2 and BEAS-2B cells were cultured in DMEM (Sigma-Aldrich) with the same supplements as above. Human PBECs were obtained using flexible fiberoptic bronchoscopy under light sedation with fentanyl and midazolam from healthy control volunteers and all participants provided written informed consent. The study was reviewed by the Oxford Research Ethics Committee B (18/SC/0361). Airway epithelial cells were cultured in Airway Epithelial Cell medium (PromoCell, Heidelberg, Germany) in submerged culture. PBECs were cultured on PureCol-coated 0.4 μ m pore polyester membrane permeable inserts (Corning) in serum-free airway epithelial cell media, brought to air-liquid interface, replacing basal media with ALI media (StemCell Pneumacult). The media was exchanged every 2 days and apical surfaces washed with PBS weekly to disperse accumulated mucus for at least 6 weeks.

METHOD DETAILS

Reagents

Real-time luciferase activity was acquired at 30 min intervals using a ClarioStar plate reader (BMG). HEK293T cells stably expressing Lenti-rLuc-GFP 1–7 and RSV-F protein, or separately, Lenti-rLuc-GFP 8–11, were used for fusion assays and maintained using DMEM (Sigma-Aldrich) supplemented with 10% FBS (Life Technologies Ltd), 1% Na Pyruvate (Sigma-Aldrich) and 1% Pen-Strep (10000 U ml^{−1}; Life Technologies Ltd). Daprodustat (GSK: 1278863), Molidustat (Bay 85-3934), Roxadustat (FG-4592) were obtained from MedChemExpress. For IH the following antibodies were used: goat anti-RSV (AB1128; Millipore), goat-HRP (ab6741; Abcam) and Envision+System HRP Rabbit (K4003; Agilent Dako).

siRNA silencing

Silencing RNA for NCL (human NCL silencer select) and siRNA controls were obtained from Thermo Fisher. For siRNA-mediated silencing, NCL siRNA or a scrambled control at 25 nM were transfected using DharmaFECT 4 (Thermo Fisher). 24h post transfection, Calu-3 were infected with RSV-GFP and monitored using Incucyte S3 live cell imaging. 48h post transfection cells were harvested for western blotting.

Cell-cell fusion assay

HEK293T Lenti rLuc-GFP 1–7 engineered to express RSV-F (effector cells) and HEK293T Lenti rLuc-GFP 8–11 (target cells) were co-cultured in a 96-well plate in the presence of doxycycline (1 μ g/mL), to induce the expression of RSV-F by effector cells.⁸⁶ Each cell line was diluted to dispense 2x10⁴ cells/well in a final volume of 100 μ L and PHIs were added to the culture media. After 48h, GFP signal was quantified using an IncuCyte S3 live cell imaging system (Essen BioScience).

RSV infection and quantification of virus infectivity

Human RSV subtype A (A2 strain) was grown in HEp-2 cells and cell lysates were concentrated using Vivaspin® 20, 10,000 MWCO PES columns (Sartorius). In brief, cells were infected at MOI 0.2 for 2h, the inoculum was removed, cells washed with PBS and cultured in DMEM 2% containing 5% FBS. After 5 days, cells were harvested and cellular lysates clarified and concentrated using Vivaspin® 20. The aliquoted viral stock was snap frozen in liquid nitrogen and stored at -80°C.

Calu-3, HEp-2 or BEAS-2B cells were infected with RSV at an MOI of 0.2 for 2h, the viral inocula removed by washing the cells three times in PBS and the cultures maintained in growth media. PBEC-ALI cultures were washed with PBS and infected apically with RSV-A2 (an estimated MOI of 5) for 2h at 37°C. Daprodustat was added in the basal medium and shed virus harvested at 48hpi by washing the cultures with 50 μ L of medium followed by a standard focus forming assay using HEp-2 cells. For viral kinetics, Calu-3 were seeded at 5x10⁴ cells/well in a clear flat-bottomed 96 well-plate. Cells were allowed to grow to 80% confluence, and infected with RSV-GFP. After removal of the inoculum, plates were imaged every 8h using an IncuCyte S3 live cell imaging system. GFP expression was determined using the total integrated intensity metric function in the IncuCyte S3 software.

Samples from infected cells and lung homogenates from infected mice were serially diluted 1:10 and used to inoculate monolayers of HEp-2 cells for 2h. Inocula were removed and replaced with DMEM containing 1% FCS with a semi-solid overlay consisting of 1.5% carboxymethyl cellulose (Sigma-Aldrich). Cells were incubated for 4-5 days, after which cells were fixed in 4% PFA, stained with 0.2% crystal violet (w/v) and visible plaques enumerated, where the limit of detection of this assay was 10 focus forming units (FFU)/mL.

RSV minigenome

Calu-3 cells were seeded in 24-well plates, inoculated with Fowlpox-T7 and the following day transfected with plasmids encoding the RSV replicase: phosphoprotein (P); nucleoprotein (N); polymerase (L); anti-transcription-termination factor (M2-1) and a subgenomic human RSV A2 luciferase replicon.³⁸ Transfected cells were cultured at 37°C for 24 h, treated with drugs and 48h later lysed and luciferase determined as a measure of hRSV replication and transcription.

qPCR quantification

Viral RNA was extracted from infected cells using a RNeasy kit (Qiagen) according to the manufacturer's instructions. Lung tissue from infected mice were homogenised in Trizol and extracted according to the manufacturer's instructions. Viral or cellular RNA was determined by qPCR using a Roche Light Cyclers 96.

Immunoblotting

Cell lysates were prepared by washing cells with phosphate buffered saline (PBS), then lysed in lgepal lysis buffer (10mM Tris pH 7.5, 0.25M NaCl, 0.5% lgepal) supplemented with Complete™ protease inhibitor cocktail (Roche) at 4°C for 5 min, followed by clarification by centrifugation (3 min, 12,000 rpm). Supernatant was mixed with Laemmli sample buffer and boiled at 100°C, separated by SDS-PAGE and proteins transferred to polyvinylidene difluoride membrane (Immobilon-P, Millipore). Membranes were blocked in 5% milk in PBS/ 0.1% Tween-20, incubated with anti-HIF-1 α (BD Transduction Laboratories, clone#610959), anti-NCL (abcam, clone# 22758), anti-NDRG1 (Cell signaling, clone#5196) or anti- β -actin (Sigma, clone#A5441) primary antibodies and appropriate HRP-conjugated secondary Mouse antibodies (DAKO, clone#P0447) and Rabbit antibodies (Cytiva, clone#NA934V). Chemiluminescence substrate (West Dura, 34076, Thermo Fisher Scientific) was used to visualize proteins using a ChemiDoc XRS+ imaging system (BioRad). Densitometric analysis was performed using ImageJ software (NIH).

Flow cytometry

HEK293T effector cells were plated in a 12 well-plate in presence of PHI and doxycycline. The following day, they were stained with an APC conjugated anti-RSV-F antibody and with LIVE/Dead™ Fixable Aqua (Life Technologies) for 30 min at 4°C. Cells were analysed on a MACSQuant Analyzer flow cytometer (Miltenyi Biotec) and data analyzed using FlowJo (TreeStar). HEp-2 or Calu-3 cells were seeded in a 6 well-plate and incubated with Daprodustat (50 mM or 100 mM) for 48h. Cells were trypsinised, stained with LIVE/Dead™ Fixable Aqua (Life Technologies), permeabilized for 15min at room temperature (0.1% Triton X-100 in PBS), fixed with 4% paraformaldehyde (PFA, Sigma) for 10min at room temperature and blocked for 20min on ice (0.5% BSA, 0.5% tween in PBS). Cells were stained in darkness with primary nucleolin antibody (abcam, ab129200) for 20 min on ice, followed by staining with in fluorescent dye conjugated secondary antibody (goat anti-rabbit Alexa 488nm, Thermo Fisher, A11034) for 20min on ice. Data was acquired using an Attune NxT flow cytometer (Thermo Fisher) and analyzed using FlowJo (TreeStar).

Confocal immunofluorescence microscopy

Infected cells were fixed with 4% paraformaldehyde (PFA; Sigma) in PBS for 15 min, blocked with 20mM glycine in PBS and permeabilized with 0.5% Triton X-100 in PBS for 5 min. Cells were incubated with anti-RSV-F primary antibody for 1h at room temperature. After incubation, they were washed and incubated with Alexa Fluor secondary antibodies (Life Technologies) for 1h at room temperature. After washing, slides were mounted with Fluoromount G (SouthernBiotech) containing 4',6-diamidino-2-phenylindole (DAPI) for nuclei staining. Cells were imaged on a Leica TCS SP5 confocal microscope using the 488-nm laser line for the appropriate dyes and a 63 \times oil immersion objective.

Animals and Daprodustat treatment

Animal work was approved by the local University of Liverpool Animal Welfare and Ethical Review Body and performed under UK Home Office Project Licence PP4715265. Female BALB/c mice (BALB/cAnNCr), 8-10 weeks of age were purchased from Charles River and maintained under SPF barrier conditions in individually ventilated cages. Mice were divided in two groups for treatment with vehicle or Daprodustat (n = 4-6 per group). Animals were treated with 10mg/kg or 30mg/kg of Daprodustat (MedChem Express) by oral gavage. Drug was dissolved in 99% double distilled H₂O, 0.5% methyl cellulose and 0.5% Tween-80, administered twice daily. Animals were euthanised on day 4 post-treatment and tissues collected for histological examination. Reticulocyte counts were quantified by staining terminal blood samples with 0.1% Brilliant Cresyl Blue.

RSV-Daprodustat challenge experiments

Two identical experiments were performed. For both, female BALB/c mice (8-10 weeks old) were randomly assigned into cohorts (4 or 6 animals). Daprodustat (30mg/kg)/vehicle treatment commenced 24h prior to infection and was maintained until termination of the study 4 days post infection. For infection, mice were anaesthetized lightly with KETASET i.m. and inoculated with 1 \times 10⁷ PFU of RSV-A2 strain. Viral inocula were made in sterile PBS and delivered via intranasal instillation (50 μ L total per mouse). Animal weights were monitored daily and visual inspection of all animals carried out twice daily. Animals were euthanised at day 4 post infection and lungs dissected at necropsy for histological and immunohistological examination (left lungs) and virology assays (right lungs). Reticulocyte counts were quantified by staining terminal blood samples with 0.1% Brilliant Cresyl Blue.

Histological and immunohistological examination

The left lungs were fixed in 10% buffered formalin for 48h and stored in 70% ethanol until processing. Lungs were trimmed (longitudinal section) and routinely embedded in paraffin wax. Consecutive sections (3 μ m) were prepared and stained with haematoxylin eosin (HE) for histological assessment and subjected to immunohistology (IH) for the detection of RSV antigen. IH was performed using the horseradish peroxidase (HRP) method. Briefly, after deparaffination, sections underwent antigen retrieval in Tris/EDTA buffer (pH 9) for 20 min at 98°C, followed by incubation with goat anti-RSV (Millipore) diluted in dilution buffer (Agilent Dako) overnight at 4°C. This was followed by blocking of endogenous peroxidase (peroxidase block, Agilent Dako) for 10 min at room temperature (RT) and incubation with goat HRP (Abcam) for 30 min at RT, all in an autostainer (Agilent Dako). Sections were counterstained with haematoxylin. A formalin fixed and paraffin embedded RSV infected (MOI 0.2, 48 hpi) Calu-3 pellet served as positive control; tissue sections incubated without the primary antibody served as negative

controls. Further sections were stained for Iba1 (monocytes/macrophage marker), CD3 (T cell marker) and Ly6G (neutrophil marker) following established protocols.^{83,87}

RNA-sequencing analysis

Total cellular RNAs were prepared as described above and sequenced using 300bp paired end Illumina sequencing (Novogene, UK). Host reads were mapped to the human transcriptome and differential expression analysis performed using DESeq2. Pathway analyses were performed using Gene Set Enrichment Analysis (GSEA 4.1.0), and the Hallmarks gene sets from the Molecular Signatures Database.

QUANTIFICATION AND STATISTICAL ANALYSIS

All data are presented as mean values \pm SEM. P values were determined using a Mann-Whitney test (two group comparisons) or with a Kruskal–Wallis ANOVA (multi group comparisons) using PRISM version 8. In the figures * denotes $p < 0.05$, ** < 0.01 , *** < 0.001 and **** < 0.0001 .